



Viscosity and Interfacial Tension of Binary Mixtures Consisting of an *n*-Alkane, Branched Alkane, Primary Alcohol, or Branched Alcohol and a Dissolved Gas Using Equilibrium Molecular Dynamics Simulations

Chathura J. Kankanamge¹ · Frances D. Lenahan¹ · Tobias Klein¹ · Andreas P. Fröba¹

Received: 1 April 2022 / Accepted: 3 May 2022 / Published online: 27 May 2022
© The Author(s) 2022

Abstract

This study aims to characterize binary mixtures consisting of a liquid with a dissolved gas by determining their dynamic viscosity and interfacial tension using equilibrium molecular dynamics (EMD) simulations in the temperature range between (298 and 573) K and for solute mole fractions up to 0.20. With the help of a systematic variation of solvent and solute molecules, the influence of their molecular characteristics, e.g., in form of size, shape, or polarity, on the thermophysical properties of the mixtures is discussed. For this, eight different alkanes and alcohols with a carbon number between 12 and 40 as solvents and seven solutes in form of hydrogen, helium, methane, water, nitrogen, carbon monoxide, or carbon dioxide are studied. Using EMD simulations, the liquid dynamic viscosity is determined in the slightly compressed liquid phase close to saturation conditions. Simulations at vapor–liquid-equilibrium (VLE) are performed to determine the interfacial tension and to calculate the solute molecules at the vapor–liquid interface. To check the applicability of the EMD simulations, data for the dynamic viscosity and interfacial tension from this work are compared to experimental data of binary mixtures with the same solutes and similar solvents. The results from this work show that the impact of the dissolved gas on the thermophysical properties is strongly depending on its molecular characteristics. For example, the properties of mixtures containing dissolved He are usually within combined uncertainties with the ones of the pure solvent. In contrast, dissolving CO₂ leads to a pronounced reduction in both properties at comparable solute mole fractions. For the molecular characteristics of the solvent, the carbon chain length is shown to influence mainly the interfacial tension and the polarity mainly influences the viscosity.

Keywords Binary mixtures · Gases · Hydrocarbons · Interfacial tension · Molecular dynamics simulations · Viscosity

1 Introduction

Mixtures consisting of liquids with dissolved gases are often in use as working fluids in many processes in chemical and energy engineering. Examples are the synthesis of base chemical components, such as methanol [1, 2] or dimethyl ether [2, 3], the conversion of carbon dioxide (CO₂) and water to synthesis gas [4], or the esterification of biofuels [5, 6]. For the efficient design of processes and apparatuses, reliable data for the thermophysical properties of the working fluid is needed at process-relevant conditions in terms of temperature T , pressure p , and composition. Two important properties are the dynamic viscosity η and interfacial tension σ , which are addressed within this work. For example, η is related to the momentum transport and, therefore, required for the calculation of power requirements for mixers and pumps and the characterization of the flow field in pipes and reactors. σ is important for describing the wetting behavior at catalysts or machineries and the mass transfer at gas–liquid interfaces.

Due to the infinite number of combinations of solvents, solutes, and thermodynamic states, the investigation of η and σ only by experiments is not a feasible task. For systems which cannot or only hardly be probed by experiments, also because of safety reasons, the use of computer simulations has proven to be a valuable tool for thermophysical property research.

Equilibrium molecular dynamics (EMD) simulations, which are used in this work for the determination of η and σ , are based on the study of the molecular motion in a statistical fluid ensemble by solving Newton's equations of motion using descriptions of the intra- and intermolecular interactions via so-called force fields (FF) [7–9]. In this way, multiple thermophysical properties can be calculated from the recorded molecule trajectories and energies. A further advantage of EMD simulations is the possibility to gain insight into the fluid structure on a molecular level which is valuable for the analysis of structure–property relationships and can be utilized for the development of prediction models [10–12].

The present work is part of a research project at the Institute of Advanced Optical Technologies-Thermophysical Properties (AOT-TP) at the Friedrich-Alexander-Universität Erlangen-Nürnberg (FAU). The project aims at the characterization of pure linear, branched, or cyclic hydrocarbons and their mixtures without and with dissolved gases by the determination of η and surface or interfacial tension σ over a wide range of thermodynamic states via surface light scattering (SLS) experiments and EMD simulations. In a first step, a T -dependent modification of the L-OPLS FF [13, 14] served for improved predictions of the liquid density ρ_L , η_L , and σ of 12 pure solvents up to $T=573$ K [15]. This modification has since been applied to binary liquid mixtures of n -hexadecane with n -octacosane, 2,2,4,4,6,8,8-heptamethylnonane (HMN), or 1-hexadecanol [16], and binary mixtures consisting of long linear, branched, or cyclic hydrocarbons and seven different gases between (303 and 573) K [17, 18]. For all investigations, the results of EMD simulations could be directly compared with the SLS experiments. Here again, EMD simulations are used to determine η_L and σ of 45 further binary mixtures consisting of a liquid with a dissolved gas up to $T=573$ K

and mole fractions of the dissolved gas in the liquid phase up to 0.20. As solvents, linear and branched alkanes and alcohols of varying carbon number are investigated to cover a wide range of molecular size and weight as well as polarity. In detail, *n*-dodecane, 1-dodecanol, 2-butyl-1-octanol, HMN, 1-hexadecanol, *n*-octacosane, 2,6,10,15,19,23-hexamethyltetracosane (squalane), and *n*-tetracontane are selected as solvents. As solutes, hydrogen (H₂), helium (He), methane (CH₄), water (H₂O), nitrogen (N₂), carbon monoxide (CO), and CO₂ were chosen for their variety in size, weight, sphericity, and polarity.

In the following, the relevant information for the EMD simulations, including the applied FFs, simulation procedure, and data evaluation will be given. Afterwards, the influence of the molecular characteristics of the solvent and solute on the thermophysical properties of the mixtures is discussed. The influence of the solute is analyzed by comparing the results for binary mixtures consisting of different gases dissolved in either *n*-dodecane, 1-dodecanol, or *n*-tetracontane. The simulation results are compared to experimental data. Because of the scarce data situation in the literature, results for similar systems are used for comparison purpose mainly with results for binary mixtures based on similar solvents from our previous investigations [17, 18]. The influence of the solvent is analyzed by comparing the results for binary mixtures consisting of the solutes He, N₂, or CO₂ dissolved in various solvents. Finally, the enrichment of solute molecules at the vapor–liquid interface is calculated via the relative adsorption $\Gamma_2^{(1)}$ and related to the results for σ to deepen the understanding why different solute types have a different impact on σ of the binary mixtures.

2 EMD Simulations

EMD simulations predict the movement of atoms and molecules in a statistical ensemble by solving Newton's classical equations of motions and describing the intra- and intermolecular interactions between two atoms. From the resulting trajectories, forces, and energies, a broad range of thermophysical properties, including the viscosity and interfacial tension which are of interest in this work, can be accessed. Further information on the underlining principals of MD simulations can be found in the respective literatures [7–9]. In the following, only the relevant information of the present study is summarized.

The accuracy of the predicted properties from EMD simulations strongly depends on the employed FFs. The L-OPLS FF was chosen for modeling of the solvent molecules, since it has shown the best agreement with experimental reference data for predicting equilibrium and transport properties of long alkanes and alcohols [19], including diffusivities in their mixtures with dissolved gases [10, 11, 20–22].

In our previous studies, by incorporating a *T* dependency in one parameter of the 6–12 Lennard–Jones (LJ) potential, which is used to describe repulsive and dispersive interactions between two atoms, the L-OPLS all-atom (AA) FF [13, 14] was modified for a better representation of the density ρ , η , and σ of 12 pure linear or branched alkanes and alcohols with carbon numbers between 12 and 40 at *T* between (298.15 and 573.15) K [15]. This modification led to improved predictions of ρ , η ,

and σ with average absolute relative deviations from SLS experiments, which were presented in the same work, of (1.1, 17, and 11) %, respectively. The T -dependent modification [15], which is fully transferable to other substances, was then tested by comparing predicted η and σ of binary liquid mixtures of linear and branched alkanes and alcohols [16], cyclic liquid organic hydrogen carriers (LOHCs) [23] and their mixtures [24] as well as binary mixtures consisting of a hydrocarbon liquid with different dissolved gases [17, 18] to experimental values from SLS. In all cases, the T -dependent modification has shown to greatly improve the T -dependent drift of the simulated properties in comparison to the experimental ones. Therefore, the same FFs are employed within this study for the solvent molecules. The partial charges located on the center of the atoms were taken from the original publications and are summarized together with the FF parameters in the Supporting Information of our previous publication [15]. For the gas solutes, namely, H_2 , He, CH_4 , H_2O , CO, N_2 and CO_2 , the FFs employed in our previous publications are used [17, 18]. All FFs used in this study are non-polarizable flexible all atom FFs, characterized by pair-additive potential energy functions describing intramolecular and intermolecular interactions.

2.1 Simulation Details

All EMD simulations were performed using the GROMACS software package, version 5.1.2 [25] at $T=(298.15, 323.15, 348.15, 373.15, 423.15, 473.15$ and $573.15)$ K or starting at elevated T for solvents with a melting T above 298.15 K. Equations of motion were integrated using the Leapfrog algorithm with an integration time step of 2 fs for all systems. The bonds between the lighter hydrogen atoms and the heavier carbon or oxygen atoms in the solvent molecules were constrained using the LINCS [26] algorithm. The LJ and electrostatic interactions are calculated from the 6–12 LJ potential and coulombic potential, within the cutoff radius of 1.6 nm. Long-range electrostatic interactions beyond the cutoff radius is modeled via the particle-mesh Ewald (PME) algorithm [27]. For simulations in the slightly compressed liquid phase, standard dispersion corrections for energy and pressure is considered for calculating long-range LJ interactions beyond the cutoff radius. Long-range LJ interaction in VLE simulations are calculated using LJ-PME algorithm [28].

The simulations were initialized by randomly inserting solvent molecules into a cubic simulation box with periodic boundary conditions in all directions. The number of solvent molecules corresponds to approximately 30,000 atoms in each case to maintain comparable computational effort for all mixtures. Three unique simulation boxes are created, which are the bases of three independent simulation runs for all following steps. Afterwards, solute molecules are added to match the calculated solubility data. Details on the solubility data used in this work are discussed in the Supporting Information. After an energy minimization step to approximate realistic atomic proximities following the random insertion of molecules into the simulation box, the desired T and p was attained in 1 ns simulation run in a canonical ensemble (NVT), followed by a 10 ns simulation run in an isothermal-isobaric ensemble (NpT). To avoid a possible phase separation, p in the NpT simulations was

set 0.2 MPa above the calculated saturation p . ρ_L was determined from the NpT simulation, neglecting first 0.5 ns for equilibration of T and p , and the liquid dynamic viscosity η_L was calculated from a subsequent simulation in an NVT ensemble based on the Green–Kubo method [29, 30], which is further detailed in the “Data evaluation” section.

To create a simulation box in VLE, which is required for calculating σ , the cubic simulation boxes were extended in the z -direction to create two vapor–liquid interfaces. For typical simulation boxes with a box length of (6.0 to 7.0) nm, previous studies have shown that an extension by a factor of three is sufficient to ensure that the long solvent molecules in the vapor phase only interact with one of the two interfaces. Additional solute gas molecules were then added to the vapor phase to reach the vapor density of the solute at the required partial pressure. These values were obtained from the REFPROP data base [31]. Afterwards, VLE simulations of about (15 to 20) ns in an NVT ensemble were performed to calculate σ , neglecting the first 5 ns for equilibration. From the same VLE simulations, the partial number densities of the solute and solvent as function of the z -coordinate of the simulation box were obtained to study a possible enrichment of the constituent species at the interface, which is further explained in Sect. 2.2.

For calculating the composition in the liquid phase and the related saturation p , solubility data are required. Experimental solubility data are only available for a few systems and had to be inter- and extrapolated with respect to the carbon number in the solvent molecules for all other systems. This is detailed in the Supporting Information.

2.2 Data Evaluation

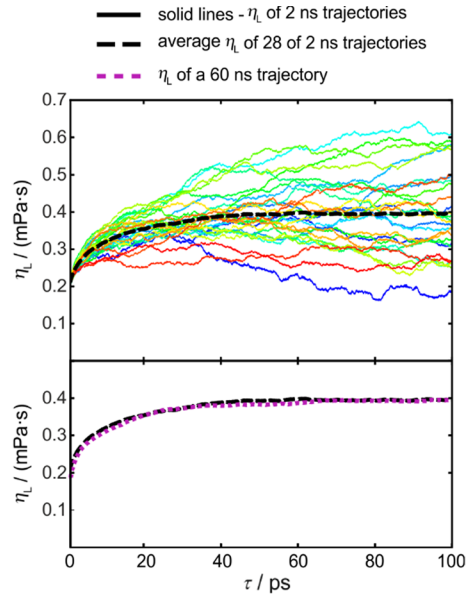
The Green–Kubo formalism [29, 30] is used to calculate η_L within this study. This formalism analyzes the pressure autocorrelation function (PACF) of the off-diagonal elements of the p tensor. By averaging over the plateau of the running integral of the PACF $\eta_L(\tau)$ with respect to correlation time τ , η_L can be obtained. However, in practice, it is difficult to identify the plateau region due to an accumulation of statistical noise at long correlation times [32]. Alternatively, Zhang et al. [33] proposed a time-decomposition method for the reliable determination of η_L . Using this method, $\eta_L(\tau)$ of multiple short simulation runs are fitted to a double exponential function according to

$$\eta_L(\tau) = A\alpha\tau_1(1 - e^{-\tau/\tau_1}) + A(1 - \alpha)\tau_2(1 - e^{-\tau/\tau_2}). \quad (1)$$

In Eq. 1, A and α are fitting parameters and τ_1 and τ_2 characterize the decay time of the two exponential functions. For more detail of this method, reader is referred to the respective publication [33]. In the following, the procedure adopted within this study is detailed.

To apply the method of Zhang et al. [33], the NVT simulations are divided into multiple short simulations of 2 ns. In the upper part of Fig. 1, $\eta_L(\tau)$ for the resulting 28 short simulations for the binary mixture of 1-dodecanol and CO_2 with $x_{\text{CO}_2} = 0.20$ at 423.15 K is shown together with their running average indicated by

Fig. 1 (Top part) Liquid dynamic viscosity η_L of 28 simulations of 2 ns length (solid lines) and their running average (dashed line) as a function of the correlation time τ for the binary mixture of 1-dodecanol with dissolved CO_2 at a CO_2 mole fraction $x_{\text{CO}_2} = 0.2$ and temperature $T = 473.15$ K. (lower part) Comparison between the running average of the 28 simulations of 2 ns length (dashed line) and the evaluation of a single 60 ns long simulation (dotted line) as a function of τ



a black dashed line. The running average is then fitted with respect to τ according to Eq. 1. In a next step, the double standard deviation, $\sigma(\eta(\tau))$, between all individual runs is calculated as a function of τ and fitted to the functional form $\sigma(\eta(\tau)) = B \cdot \tau^b$ up to a cutoff time of $\tau_{\text{cut}} = 6 \cdot \max(\tau_1, \tau_2)$, where B and b are fitting parameters. In all the investigated systems within this study, b values were between 0.6 and 0.8. In a final step, the running average is again fitted according to Eq. 1 up to τ_{cut} with a weighing function of $1/\tau^b$. η_L follows directly from the plateau value of the theoretical equation according to Eq. 1. To compare the approach of Zhang et al. [33] with the results from one long simulation run, the running average of 28 simulations of 2 ns length is compared with $\eta_L(\tau)$ from a 60 ns long simulation run for the system of 1-dodecanol with dissolved CO_2 at $x_{\text{CO}_2} = 0.20$ is shown in the lower part of Fig. 1. While both methods yield similar η_L , the method proposed by Zhang et al. [33] has the advantage that the plateau range is calculated from the decay times of the exponential functions and is, therefore, not influenced by the subjectivity of the individual, as is the case for the classical approach.

σ is calculated from the diagonal elements of the p tensor from the simulations in VLE according to

$$\sigma(t) = \frac{L_z}{2} \left(p_{zz}(t) - \frac{p_{xx}(t) + p_{yy}(t)}{2} \right) \quad (2)$$

Here, L_z is the box length in z -direction and p_{xx} , p_{yy} , and p_{zz} are the diagonal elements of the pressure tensor. σ is then determined by averaging $\sigma(t)$ over the simulation time excluding the first 5 ns for equilibration and formation of the vapor–liquid interface. For more details on the calculation of σ from MD simulations, the reader

is referred to our previous publications [15, 34] as well as the general literature on MD simulations [7–9].

For a vapor–liquid interface parallel to the x,y -plane, the relative adsorption of the solute (component 2) with respect to the solvent (component 1) $\Gamma_2^{(1)}$ can be calculated using the component number density profiles along the z -axis $\rho_i(z)$, obtained from EMD simulations in VLE according to [35, 36]

$$\Gamma_2^{(1)} = -\left(\rho_{L,2} - \rho_{V,2}\right) \int_{-\infty}^{\infty} \left[-\frac{\rho_{L,1} - \rho_1(z)}{\rho_{L,1} - \rho_{V,2}} + \frac{\rho_{L,2} - \rho_2(z)}{\rho_{L,2} - \rho_{V,2}} \right] dz \quad (3)$$

Here, $\rho_{L,i}$ and $\rho_{V,i}$ represent the bulk liquid and vapor densities of component i far away from the vapor–liquid interface. They can be calculated by averaging over $\rho_i(z)$ in the range where $\rho_i(z)$ is independent of z .

The final results for the thermophysical properties of the binary mixtures investigated in this work are summarized in Table 1 together with their statistical uncertainties and thermodynamic states. The final values for the properties are the averages of the three independent simulation runs. The expanded statistical uncertainties, based on a coverage factor $k=2$, are calculated from the double standard deviations of the values from the three simulations.

3 Results and Discussion

The results for ρ_L , η_L , σ , and $\Gamma_2^{(1)}$ for the 45 binary mixtures investigated in this work are summarized together with their expanded statistical uncertainties and thermodynamic states in Table 1. Systems based on solutes with a low solubility, i.e., H_2 , He, and N_2 , were investigated at constant p of about 7.0 MPa to allow a comparison with previous publications containing binary mixtures with the same solutes [17, 18] which were conducted at a maximum $p=7.0$ MPa due to the limitations of the experimental setup. Systems with more soluble solutes, namely, CH_4 , CO, CO_2 , and H_2O , were investigated at $x_{\text{solute}}=(0.10$ and $0.20)$ in the case of CH_4 and CO_2 , $x_{\text{solute}}=(0.05$ and $0.10)$ in the case of CO, and $x_{\text{solute}}=(0.045$ and $0.09)$ in the case of H_2O . The simulations were carried out at T between (298.15 and 573.15) K, or starting from approximately 20 K above the melting T of the solvent. Due to the low solubility of H_2O in hydrocarbons at low T , the simulations with dissolved H_2O were carried out between $T=(423.15$ and $573.15)$ K. In the following, first the results for η_L and σ are shown and discussed. To investigate the influence of the dissolved gas, the deviation of the reported mixture properties from the pure solvents investigated by EMD simulations [15] are calculated. For this, η_L and σ of the pure solvents were correlated with respect to T , as detailed in the Supporting Information. Here, it must be mentioned that the a general overprediction for η_L and σ of the pure solvents by up to 30 % with respect to the T -dependent correlations from SLS results could be observed in our previous publication [15]. In this work, the influence of the dissolved gas in form of the deviation between the mixtures and the pure solvents is compared to experimental and simulated data for similar systems

Table 1 Liquid densities ρ_L and dynamic viscosities η_L in the compressed liquid phase close to saturation conditions as well as interfacial tensions σ and relative adsorptions $\Gamma_2^{(1)}$ at VLE conditions of the investigated binary mixtures

T (K)	p (MPa) ^a	x_{solute}^b	ρ_L (kg·m ⁻³)	$10^3 \cdot U_L(\rho_L)$	η_L (mPa·s)	$100 U_L(\eta_L)$	σ (mN·m ⁻¹)	$100 U_L(\sigma)$	$\Gamma_2^{(1)}$ (nm ⁻²)	$U(\Gamma_2^{(1)})$ (nm ⁻²)
<i>n</i> -Dodecane + H ₂ ($p \approx 7.0$ MPa)										
298.15	7.04	0.047	744.38	0.27	1.99	15	24.48	3.4	0.48	0.096
323.15	7.14	0.054	724.56	0.11	1.33	17	21.82	1.0	0.37	0.081
348.15	7.15	0.061	705.13	0.39	0.821	12	20.44	2.2	0.29	0.055
373.15	7.19	0.068	685.57	0.71	0.716	20	18.80	1.4	0.29	0.055
423.15	5.17	0.083	645.71	0.14	0.389	15	14.79	2.6	0.19	0.044
473.15	7.78	0.099	603.27	0.48	0.278	13	11.39	5.2	0.14	0.008
573.15	5.76	0.147	496.65	0.16	0.108	12	4.45	5.3	0.09	0.025
<i>n</i> -Dodecane + He ($p \approx 7.0$ MPa)										
298.15	7.16	0.016	748.44	0.28	1.81	14	25.41	5.6	0.06	0.028
323.15	7.16	0.021	729.10	0.41	1.43	26	23.32	0.8	0.05	0.010
348.15	7.12	0.027	710.10	0.32	0.870	15	21.53	1.9	0.03	0.022
373.15	7.27	0.032	691.48	0.22	0.704	2.2	19.39	0.5	0.03	0.046
423.15	7.09	0.046	652.65	0.22	0.440	10	15.61	1.9	0.02	0.028
473.15	7.07	0.062	611.65	0.56	0.291	7.4	11.88	2.8	0.01	0.016
573.15	7.00	0.103	512.83	0.65	0.135	20	4.77	5.0	0.00	0.010
<i>n</i> -Dodecane + CH ₄ ($x_{\text{solute}} \approx 0.10$)										
298.15	2.18	0.100	736.04	0.79	1.76	11	23.25	3.3	0.71	0.069
323.15	2.60	0.100	716.69	0.65	1.03	7.5	20.62	0.8	0.59	0.073
348.15	2.82	0.100	697.51	0.43	0.789	4.7	19.09	2.6	0.51	0.062
373.15	2.88	0.100	678.28	0.42	0.621	8.1	17.38	2.6	0.42	0.050
423.15	3.08	0.100	639.03	0.46	0.375	21	13.96	2.1	0.32	0.039
473.15	3.19	0.100	597.14	0.98	0.245	6.0	10.39	1.4	0.23	0.001
573.15	3.40	0.100	495.99	0.54	0.117	6.8	3.90	2.6	0.12	0.003

Table 1 (continued)

T (K)	p (MPa) ^a	x_{solite}^b	ρ_L (kg·m ⁻³)	$10^3 \cdot U_L(\rho_L)$	η_L (mPa·s)	$100 U_L(\eta_L)$	σ (mN·m ⁻¹)	$100 U_L(\sigma)$	$\Gamma_2^{(1)}$ (nm ⁻²)	$U(\Gamma_2^{(1)})$ (nm ⁻²)
<i>n</i> -Dodecane + CH ₄ ($x_{\text{solite}} \approx 0.20$)										
298.15	4.76	0.200	725.62	0.39	1.50	14	19.40	4.2	1.39	0.042
323.15	5.40	0.200	706.20	0.28	0.861	12	17.96	3.8	1.16	0.043
348.15	5.75	0.200	686.87	0.34	0.684	3.6	16.30	1.9	0.97	0.082
373.15	6.21	0.200	667.72	0.27	0.560	16	14.89	2.1	0.84	0.054
423.15	6.49	0.200	627.88	0.38	0.342	5.7	11.89	2.1	0.59	0.006
473.15	6.41	0.200	584.88	0.13	0.222	2.2	9.02	4.7	0.40	0.037
573.15	5.97	0.200	476.94	1.33	0.103	4.3	3.15	3.6	0.18	0.010
<i>n</i> -Dodecane + CO ($x_{\text{solite}} \approx 0.05$)										
298.15	5.48	0.050	742.47	0.37	1.92	32	21.96	5.1	0.79	0.040
323.15	3.70	0.050	723.24	0.40	1.17	20	20.17	2.4	0.64	0.052
348.15	3.99	0.050	704.22	0.13	0.909	3.4	18.88	2.5	0.48	0.021
373.15	4.34	0.050	684.97	0.73	0.622	14	17.31	2.6	0.38	0.037
423.15	2.35	0.050	645.91	0.74	0.368	1.0	13.91	2.2	0.26	0.014
473.15	0.90	0.050	604.26	0.66	0.254	16	10.67	1.2	0.19	0.009
573.15	2.17	0.050	503.14	0.70	0.118	3.4	4.28	3.0	0.08	0.006
<i>n</i> -Dodecane + CO ($x_{\text{solite}} \approx 0.10$)										
298.15	6.72	0.100	739.98	0.69	1.61	11	19.13	4.8	1.24	0.053
323.15	6.66	0.100	720.52	0.11	0.961	1.7	17.63	0.4	1.03	0.067
348.15	6.64	0.100	701.52	0.45	0.807	11	16.52	7.0	0.85	0.057
373.15	6.46	0.100	682.39	0.55	0.623	2.1	15.26	1.6	0.69	0.042
423.15	5.97	0.100	643.19	0.46	0.373	3.7	12.32	5.4	0.47	0.049
473.15	5.49	0.100	601.58	0.46	0.256	9.6	9.46	3.5	0.31	0.004
573.15	4.65	0.100	501.29	1.14	0.119	2.0	3.55	10.0	0.14	0.018

Table 1 (continued)

T (K)	p (MPa) ^a	x_{solute}^b	ρ_L (kg·m ⁻³)	$10^3 \cdot U_L(\rho_L)$	η_L (mPa·s)	$100 U_L(\eta_L)$	σ (mN·m ⁻¹)	$100 U_L(\sigma)$	$\Gamma_2^{(1)}$ (nm ⁻²)	$U(\Gamma_2^{(1)})$ (nm ⁻²)
<i>n</i> -Dodecane + N ₂ ($p \approx 7.0$ MPa)										
298.15	3.74	0.089	743.12	0.36	1.79	11	20.43	6.8	1.03	0.035
323.15	8.09	0.090	726.91	0.34	1.39	14	19.08	1.3	0.87	0.049
348.15	7.66	0.091	707.64	0.16	0.850	2.5	17.60	1.8	0.71	0.059
373.15	7.34	0.094	688.28	0.11	0.636	6.8	15.90	1.9	0.58	0.103
423.15	7.21	0.104	648.93	0.57	0.394	10	12.86	3.8	0.41	0.017
473.15	7.28	0.120	606.64	1.09	0.272	18	9.54	1.7	0.31	0.020
573.15	7.27	0.168	500.77	1.76	0.120	11	3.42	5.8	0.15	0.022
<i>n</i> -Dodecane + CO ₂ ($x_{\text{solute}} \approx 0.10$)										
298.15	1.06	0.100	749.26	0.47	1.46	13	23.89	2.2	0.68	0.084
323.15	1.08	0.100	729.26	0.26	1.21	19	21.85	3.7	0.64	0.080
348.15	1.52	0.100	709.93	0.43	0.859	7.7	19.83	4.1	0.57	0.138
373.15	1.70	0.100	690.36	0.47	0.612	2.4	17.76	1.2	0.51	0.055
423.15	1.87	0.100	650.24	0.77	0.373	1.9	13.95	2.7	0.38	0.016
473.15	2.29	0.100	607.96	1.13	0.251	2.3	10.49	2.9	0.33	0.009
573.15	3.08	0.100	506.99	2.09	0.121	3.3	3.72	7.2	0.19	0.029
<i>n</i> -Dodecane + CO ₂ ($x_{\text{solute}} \approx 0.20$)										
298.15	1.77	0.100	754.39	0.04	1.34	22	22.15	1.4	0.94	0.051
323.15	2.40	0.100	734.11	0.20	0.990	10	19.74	3.1	0.94	0.099
348.15	2.93	0.100	714.05	0.12	0.733	15	17.70	5.4	0.81	0.089
373.15	3.25	0.100	693.81	0.16	0.571	3.8	15.94	1.4	0.72	0.078
423.15	4.06	0.100	652.77	1.04	0.342	6.9	12.20	3.6	0.57	0.063
473.15	4.56	0.100	608.79	0.12	0.238	7.2	8.89	4.0	0.44	0.024
573.15	5.05	0.100	500.91	1.68	0.109	4.1	2.79	11.4	0.20	0.019

Table 1 (continued)

T (K)	p (MPa) ^a	x_{solute}^b	ρ_L (kg·m ⁻³)	$10^3 \cdot U_L(\rho_L)$	η_L (mPa·s)	$100 U_L(\eta_L)$	σ (mN·m ⁻¹)	$100 U_L(\sigma)$	$\Gamma_2^{(1)}$ (nm ⁻²)	$U(\Gamma_2^{(1)})$ (nm ⁻²)
<i>n</i> -Dodecane + H ₂ O ($x_{\text{solute}} \approx 0.045$)										
423.15	-0.12	0.046	646.85	0.47	0.395	10	15.60	2.2	0.02	0.019
473.15	0.23	0.046	602.82	1.16	0.272	21	11.79	0.5	0.01	0.006
573.15	0.98	0.046	498.12	1.89	0.116	4.0	4.72	4.2	0.01	0.014
<i>n</i> -Dodecane + H ₂ O ($x_{\text{solute}} \approx 0.090$)										
423.15	-0.10	0.091	647.38	0.49	0.402	10	15.58	2.6	0.20	0.256
473.15	0.25	0.091	603.27	1.21	0.266	7.7	11.77	1.9	0.04	0.002
573.15	1.74	0.091	489.09	3.47	0.110	9.0	4.75	7.8	0.03	0.011
1-Dodecanol + H ₂ ($p \approx 7.0$ MPa)										
323.15	6.72	0.073	805.39	1.25	6.35	29	29.94	4.2	0.41	0.030
348.15	7.07	0.071	785.20	0.21	3.32	17	24.98	11.1	0.33	0.056
373.15	7.06	0.071	765.04	0.18	1.93	5.7	23.04	2.7	0.26	0.061
423.15	7.17	0.078	723.61	0.53	0.866	23	19.85	5.2	0.20	0.032
473.15	5.94	0.089	680.48	0.35	0.452	4.6	15.31	1.5	0.15	0.013
573.15	7.11	0.117	584.44	0.70	0.191	3.5	8.27	2.3	0.10	0.040
1-Dodecanol + He ($p \approx 7.0$ MPa)										
323.15	7.00	0.013	813.49	0.57	9.09	17	31.62	4.8	0.06	0.042
348.15	7.38	0.014	793.03	1.03	3.61	29	26.72	3.3	0.04	0.027
373.15	7.15	0.018	772.67	0.45	2.10	18	24.20	2.8	0.03	0.024
423.15	7.22	0.025	732.17	0.47	0.921	11	20.77	5.2	0.02	0.029
473.15	7.03	0.038	690.15	0.44	0.479	3.6	16.44	2.7	0.01	0.006
573.15	6.04	0.072	597.55	1.11	0.203	17	8.70	1.2	0.00	0.026
1-Dodecanol + CH ₄ ($x_{\text{solute}} \approx 0.10$)										
323.15	3.03	0.100	799.90	0.65	6.16	23	26.23	10	0.64	0.118

Table 1 (continued)

T (K)	p (MPa) ^a	x_{solite}^b	ρ_L (kg·m ⁻³)	$10^3 \cdot U_L(\rho_L)$	η_L (mPa·s)	$100 U_L(\eta_L)$	σ (mN·m ⁻¹)	$100 U_L(\sigma)$	$\Gamma_2^{(1)}$ (nm ⁻²)	$U(\Gamma_2^{(1)})$ (nm ⁻²)
348.15	3.22	0.100	779.23	0.99	3.10	21	23.48	3.1	0.61	0.016
373.15	3.63	0.100	758.89	0.31	1.71	3.0	21.62	1.2	0.55	0.053
423.15	3.99	0.100	717.58	0.66	0.810	13	18.23	1.7	0.43	0.038
473.15	4.34	0.100	675.39	1.12	0.437	11	14.60	1.0	0.31	0.072
573.15	4.09	0.100	580.93	0.65	0.189	5.2	7.52	1.4	0.17	0.014
1-Dodecanol + CH ₄ ($x_{\text{solite}} \approx 0.20$)										
323.15	5.79	0.200	787.40	0.29	4.50	17	22.05	7.6	1.28	0.105
348.15	6.45	0.200	766.98	0.20	2.36	16	20.29	1.2	1.13	0.105
373.15	7.07	0.200	746.58	0.31	1.40	3.6	18.77	7.8	0.97	0.063
423.15	7.56	0.200	704.90	0.86	0.635	10	15.86	1.5	0.72	0.032
473.15	8.15	0.200	662.42	0.39	0.390	3.4	12.60	2.9	0.55	0.044
573.15	8.37	0.200	569.04	0.32	0.175	2.7	6.12	4.4	0.30	0.022
1-Dodecanol + CO ($x_{\text{solite}} \approx 0.05$)										
323.15	3.26	0.051	806.51	0.54	5.94	31	26.48	9.3	0.65	0.068
348.15	3.54	0.051	785.99	0.31	3.40	13	22.98	2.3	0.57	0.039
373.15	3.70	0.051	765.67	0.38	1.83	11	22.20	5.4	0.46	0.024
423.15	3.82	0.051	724.65	0.65	0.810	1.9	18.38	2.6	0.35	0.024
473.15	3.68	0.051	682.45	0.47	0.451	5.0	14.69	1.6	0.24	0.005
573.15	3.44	0.051	589.91	0.64	0.204	11	7.64	4.7	0.13	0.016
1-Dodecanol + CO ($x_{\text{solite}} \approx 0.10$)										
323.15	7.44	0.100	803.40	0.33	5.73	23	23.98	3.8	1.00	0.100
348.15	7.57	0.100	782.77	0.23	3.19	19	20.69	4.9	0.90	0.016
373.15	7.32	0.100	762.35	0.28	1.80	24	19.80	4.2	0.80	0.014
423.15	7.49	0.100	721.57	0.64	0.786	7.1	16.60	2.3	0.58	0.053

Table 1 (continued)

T (K)	p (MPa) ^a	x_{solite}^b	ρ_L (kg·m ⁻³)	$10^3 \cdot U_L(\rho_L)$	η_L (mPa·s)	$100 U_L(\eta_L)$	σ (mN·m ⁻¹)	$100 U_L(\sigma)$	$\Gamma_2^{(1)}$ (nm ⁻²)	$U(\Gamma_2^{(1)})$ (nm ⁻²)
473.15	7.25	0.100	679.71	0.37	0.439	9.4	13.04	0.4	0.41	0.050
573.15	8.68	0.100	588.98	0.53	0.206	5.4	6.56	1.1	0.22	0.039
1-Dodecanol + N ₂ ($p \approx 7.0$ MPa)										
323.15	8.62	0.042	813.00	1.40	7.31	28	26.77	6.7	0.78	0.055
348.15	7.42	0.045	791.51	0.38	2.85	7.2	23.06	3.0	0.71	0.021
373.15	7.51	0.048	771.22	0.12	1.92	24	21.36	6.2	0.56	0.020
423.15	7.19	0.059	729.82	0.17	0.896	11	17.75	4.3	0.43	0.008
473.15	7.14	0.073	687.19	0.15	0.469	10	14.27	2.8	0.31	0.035
573.15	6.19	0.110	592.27	0.76	0.197	9.7	6.87	2.1	0.17	0.003
1-Dodecanol + CO ₂ ($x_{\text{solite}} \approx 0.10$)										
323.15	1.60	0.100	813.48	0.90	4.65	0.70	26.59	5.2	0.47	0.109
348.15	2.09	0.100	792.54	0.28	2.66	16	24.33	4.6	0.51	0.082
373.15	1.93	0.100	771.53	0.09	1.75	18	22.26	5.5	0.50	0.056
423.15	2.33	0.100	729.52	0.20	0.838	8.2	18.43	2.9	0.40	0.061
473.15	2.69	0.100	686.41	0.67	0.450	14	14.65	3.9	0.30	0.038
573.15	2.79	0.100	589.73	0.30	0.195	12	7.27	6.8	0.17	0.023
1-Dodecanol + CO ₂ ($x_{\text{solite}} \approx 0.20$)										
323.15	2.72	0.200	817.05	0.66	4.52	11	23.37	4.1	1.19	0.227
348.15	3.44	0.200	795.92	0.62	2.12	26	21.28	1.2	1.07	0.206
373.15	3.86	0.200	774.67	0.64	1.28	16	19.70	2.4	1.00	0.107
423.15	4.79	0.200	731.89	0.24	0.649	9.6	16.10	0.7	0.75	0.105
473.15	5.14	0.200	687.43	0.56	0.403	2.8	12.60	3.5	0.56	0.020
573.15	4.73	0.200	588.19	0.32	0.172	2.7	5.87	5.3	0.31	0.011

Table 1 (continued)

<i>T</i> (K)	<i>p</i> (MPa) ^a	<i>x</i> _{solite} ^b	ρ_L (kg·m ⁻³)	$10^3 \cdot U_L(\rho_L)$	η_L (mPa·s)	$100 U_L(\eta_L)$	σ (mN·m ⁻¹)	$100 U_L(\sigma)$	$\Gamma_2^{(1)}$ (nm ⁻²)	$U(\Gamma_2^{(1)})$ (nm ⁻²)
1-Dodecanol + H ₂ O (<i>x</i> _{solite} ≈ 0.045)										
423.15	0.17	0.046	727.66	0.48	0.841	4.6	20.73	2.3	0.02	0.015
473.15	0.25	0.046	684.64	0.22	0.481	8.0	16.59	0.8	0.01	0.037
573.15	0.72	0.046	588.77	1.02	0.194	4.8	8.55	2.8	0.02	0.006
1-Dodecanol + H ₂ O (<i>x</i> _{solite} ≈ 0.090)										
423.15	0.07	0.091	727.96	0.51	0.875	14	20.67	1.4	0.07	0.036
473.15	0.24	0.091	684.33	0.97	0.486	6.6	16.42	1.9	0.03	0.010
573.15	1.02	0.091	586.37	0.62	0.193	10	8.27	2.7	0.05	0.010
<i>n</i> -Tetracontane + H ₂ (<i>p</i> ≈ 7.0 MPa)										
423.15	7.14	0.146	737.41	0.49	3.13	20	23.73	3.2	0.21	0.040
473.15	7.07	0.169	704.79	0.35	1.81	25	20.53	1.9	0.16	0.038
573.15	5.80	0.217	638.35	0.73	0.982	11	14.59	4.4	0.09	0.036
<i>n</i> -Tetracontane + He (<i>p</i> ≈ 7.0 MPa)										
423.15	6.93	0.050	742.54	0.34	3.21	24	24.38	4.3	0.00	0.010
473.15	7.06	0.065	711.34	1.11	2.64	19	21.66	2.3	0.01	0.014
573.15	7.15	0.109	647.87	0.68	0.954	12	15.36	2.5	0.01	0.006
<i>n</i> -Tetracontane + CH ₄ (<i>x</i> _{solite} ≈ 0.10)										
423.15	1.29	0.103	734.97	1.22	3.17	27	23.68	4.7	0.16	0.029
473.15	1.55	0.103	703.13	0.92	1.85	10	20.65	2.4	0.12	0.026
573.15	1.64	0.103	638.10	0.59	0.953	13	15.18	2.4	0.07	0.004
<i>n</i> -Tetracontane + CH ₄ (<i>x</i> _{solite} ≈ 0.20)										
423.15	3.09	0.202	731.17	0.23	2.48	25	23.35	1.3	0.31	0.009
473.15	3.08	0.202	698.88	0.37	1.66	24	20.18	4.4	0.23	0.005
573.15	3.21	0.202	633.69	0.21	0.949	17	14.45	1.7	0.14	0.018

Table 1 (continued)

T (K)	p (MPa) ^a	x_{solite}^b	ρ_L (kg·m ⁻³)	$10^3 \cdot U_L(\rho_L)$	η_L (mPa·s)	$100 U_L(\eta_L)$	σ (mN·m ⁻¹)	$100 U_L(\sigma)$	$\Gamma_2^{(1)}$ (nm ⁻²)	$U(\Gamma_2^{(1)})$ (nm ⁻²)
<i>n</i> -Tetracontane + CO ($x_{\text{solite}} \approx 0.05$)										
423.15	1.89	0.050	737.96	0.63	2.47	11	23.63	6.5	0.18	0.019
473.15	1.74	0.050	706.00	0.32	2.17	18	20.92	2.9	0.11	0.025
573.15	1.26	0.050	640.64	0.18	0.949	15	15.24	4.7	0.05	0.019
<i>n</i> -Tetracontane + CO ($x_{\text{solite}} \approx 0.10$)										
423.15	3.68	0.103	737.20	0.43	2.67	25	23.21	4.2	0.33	0.033
473.15	3.34	0.103	705.11	0.68	1.95	17	20.04	5.0	0.23	0.015
573.15	2.67	0.103	639.83	0.24	0.892	13	14.82	1.3	0.10	0.016
<i>n</i> -Tetracontane + N ₂ ($p \approx 7.0$ MPa)										
423.15	7.19	0.225	737.63	1.21	3.15	6.2	21.45	6.7	0.44	0.037
473.15	7.11	0.246	704.85	0.16	2.10	32	18.85	2.8	0.32	0.014
573.15	7.95	0.277	638.69	0.31	0.922	19	13.91	3.9	0.19	0.040
<i>n</i> -Tetracontane + H ₂ O ($x_{\text{solite}} \approx 0.045$)										
423.15	0.01	0.047	737.53	0.96	2.68	25	25.38	4.4	0.01	0.009
473.15	-0.06	0.047	705.03	0.39	1.83	11	22.08	4.0	0.01	0.015
573.15	0.64	0.047	640.54	1.09	0.949	13	14.40	5.6	0.01	0.005
<i>n</i> -Tetracontane + H ₂ O ($x_{\text{solite}} \approx 0.090$)										
423.15	0.21	0.093	737.62	0.52	2.66	16	25.18	3.5	-0.01	0.042
473.15	0.08	0.093	704.21	1.47	1.65	3.4	21.35	7.5	0.02	0.009
573.15	0.87	0.093	639.11	0.47	0.954	17	15.27	3.2	0.03	0.007
Squalane + CO ₂ ($x_{\text{solite}} \approx 0.10$)										
298.15	0.50	0.102	803.12	1.10	18.7	24	28.64	14.3	0.22	0.031
323.15	0.26	0.102	785.63	0.22	7.87	14	25.60	11.2	0.21	0.088
348.15	0.67	0.102	768.81	0.18	4.16	8.0	24.56	3.0	0.21	0.039
373.15	0.86	0.102	752.05	0.65	2.94	24	21.85	4.0	0.19	0.059

Table 1 (continued)

T (K)	p (MPa) ^a	x_{solite}^b	ρ_L (kg·m ⁻³)	$10^3 \cdot U_L(\rho_L)$	η_L (mPa·s)	$100 U_L(\eta_L)$	σ (mN·m ⁻¹)	$100 U_L(\sigma)$	$\Gamma_2^{(1)}$ (nm ⁻²)	$U(\Gamma_2^{(1)})$ (nm ⁻²)
423.15	1.00	0.102	718.49	0.61	1.56	6.8	18.79	2.2	0.15	0.018
473.15	1.29	0.102	684.72	0.24	0.930	25	15.94	6.0	0.13	0.024
573.15	1.60	0.102	612.46	0.84	0.412	16	10.21	3.7	0.09	0.011
Squalane + CO ₂ ($x_{\text{solite}} \approx 0.20$)										
298.15	1.00	0.201	805.10	0.16	14.4	3.9	26.47	10.7	0.48	0.065
323.15	1.21	0.201	787.66	0.08	6.54	18	24.46	12.3	0.47	0.055
348.15	1.54	0.201	770.53	0.29	3.90	15	22.35	5.2	0.43	0.060
373.15	1.57	0.201	753.26	0.47	2.76	31	21.10	4.2	0.40	0.071
423.15	2.17	0.201	719.41	0.74	1.28	6.5	17.69	2.5	0.29	0.025
473.15	2.59	0.201	685.03	0.92	0.890	13	15.09	1.7	0.25	0.037
573.15	3.06	0.201	611.57	0.22	0.372	17	9.64	2.5	0.16	0.026
<i>n</i> -Octacosane + He ($p \approx 7.0$ MPa)										
423.15	7.03	0.049	725.73	0.69	2.07	28	22.90	2.9	0.02	0.006
473.15	7.03	0.065	693.07	0.30	1.47	17	19.77	5.4	0.01	0.012
573.15	7.04	0.108	624.82	0.82	0.555	16	12.88	3.7	0.00	0.011
<i>n</i> -Octacosane + N ₂ ($p \approx 7.0$ MPa)										
423.15	7.44	0.161	722.07	0.77	1.76	30	19.67	2.0	0.43	0.031
473.15	7.21	0.185	687.83	0.59	1.21	14	17.12	4.9	0.32	0.039
573.15	7.17	0.237	615.30	0.74	0.524	16	11.63	5.3	0.19	0.014
1-Hexadecanol + He ($p \approx 7.0$ MPa)										
348.15	7.12	0.010	794.22	0.38	4.74	28	25.76	5.0	0.03	0.026
373.15	7.08	0.010	775.44	0.30	2.42	20	23.51	4.4	0.03	0.024
423.15	7.25	0.034	736.31	0.22	1.03	4.2	19.77	3.4	0.01	0.009
473.15	4.63	0.081	690.31	0.35	0.530	12	16.46	1.9	0.01	0.010

Table 1 (continued)

T (K)	p (MPa) ^a	x_{solite}^b	ρ_L (kg·m ⁻³)	$10^3 \cdot U_L(\rho_L)$	η_L (mPa·s)	$100 U_L(\eta_L)$	σ (mN·m ⁻¹)	$100 U_L(\sigma)$	$\Gamma_2^{(1)}$ (nm ⁻²)	$U(\Gamma_2^{(1)})$ (nm ⁻²)
	5.75	0.213	582.21	0.40	0.201	13	9.34	1.3	0.01	0.011
1-Hexadecanol+N ₂ ($p \approx 7.0$ MPa)										
573.15										
348.15	7.54	0.056	792.53	0.82	3.89	15	21.46	5.2	0.69	0.047
373.15	7.25	0.056	773.30	0.46	2.14	25	19.92	0.5	0.57	0.044
423.15	7.13	0.071	734.30	0.54	0.974	15	17.19	4.9	0.42	0.067
473.15	4.78	0.095	690.69	0.60	0.511	4.4	14.03	3.1	0.29	0.011
573.15	5.55	0.162	597.90	1.72	0.217	5.6	7.70	2.9	0.18	0.018
1-Hexadecanol+CO ₂ ($x_{\text{solite}} \approx 0.10$)										
348.15	1.11	0.100	792.18	0.49	3.74	25	23.75	3.9	0.40	0.063
373.15	1.52	0.100	772.58	0.52	1.82	12	21.93	1.9	0.35	0.060
423.15	1.70	0.100	733.01	0.18	0.884	5.1	18.56	3.4	0.25	0.070
473.15	2.21	0.100	693.51	0.43	0.531	13	14.98	3.7	0.21	0.047
573.15	2.62	0.100	607.42	0.28	0.230	4.6	8.30	2.7	0.15	0.019
1-Hexadecanol+CO ₂ ($x_{\text{solite}} \approx 0.20$)										
348.15	2.86	0.201	795.22	0.38	2.90	13	21.12	7.5	0.79	0.193
373.15	2.95	0.201	774.97	0.71	1.76	27	20.35	3.8	0.71	0.216
423.15	3.73	0.201	734.91	0.25	0.838	14	16.66	5.6	0.56	0.084
473.15	4.26	0.201	694.34	0.41	0.477	13	13.17	0.5	0.45	0.043
573.15	5.10	0.201	606.68	0.59	0.211	3.8	6.94	2.5	0.28	0.052
HMN+N ₂ ($p \approx 7.0$ MPa)										
298.15	4.38	0.091	786.32	0.64	3.45	27	20.01	0.8	1.06	0.086
323.15	4.64	0.095	769.45	0.98	2.07	23	18.93	2.7	0.83	0.013
348.15	4.51	0.095	752.58	0.27	1.39	21	18.09	1.9	0.67	0.011
373.15	8.45	0.095	739.90	2.49	1.16	1.3	16.79	2.5	0.56	0.025

Table 1 (continued)

T (K)	p (MPa) ^a	x_{solite}^b	ρ_L (kg·m ⁻³)	$10^3 \cdot U_L(\rho_L)$	η_L (mPa·s)	$100 U_L(\eta_L)$	σ (mN·m ⁻¹)	$100 U_L(\sigma)$	$\Gamma_2^{(1)}$ (nm ⁻²)	$U(\Gamma_2^{(1)})$ (nm ⁻²)
423.15	7.54	0.095	705.87	0.24	0.657	9.3	14.00	4.8	0.40	0.023
473.15	7.40	0.125	668.28	0.22	0.411	3.4	11.17	5.1	0.30	0.018
573.15	7.23	0.137	589.28	0.57	0.210	9.8	6.03	4.7	0.17	0.033
HMN + CO ₂ ($x_{\text{solite}} \approx 0.10$)										
298.15	0.85	0.100	790.12	0.32	3.31	2.4	24.05	2.8	0.33	0.106
323.15	1.05	0.100	773.01	0.35	1.93	8.6	21.89	3.2	0.33	0.014
348.15	1.32	0.100	756.15	0.59	1.36	8.0	20.21	5.4	0.32	0.059
373.15	1.42	0.100	739.05	0.63	1.05	9.4	18.57	4.9	0.33	0.089
423.15	1.74	0.100	704.43	0.31	0.629	4.1	15.66	3.3	0.24	0.083
473.15	2.01	0.100	668.40	0.46	0.402	4.0	12.53	4.1	0.20	0.024
573.15	2.45	0.100	586.11	0.94	0.203	2.5	6.68	4.1	0.13	0.035
HMN + CO ₂ ($x_{\text{solite}} \approx 0.20$)										
298.15	1.69	0.201	793.55	0.48	2.50	20	23.17	3.5	0.77	0.055
323.15	2.21	0.201	775.94	0.43	1.77	21	20.52	2.2	0.72	0.165
348.15	2.58	0.201	758.49	0.35	1.15	6.4	18.98	5.9	0.72	0.155
373.15	2.90	0.201	740.95	0.18	0.877	2.7	16.78	0.8	0.62	0.099
423.15	3.45	0.201	705.12	0.36	0.550	9.2	14.07	5.3	0.50	0.024
473.15	3.94	0.201	667.71	0.26	0.379	4.5	11.04	4.7	0.39	0.009
573.15	4.60	0.201	581.80	1.06	0.180	1.3	5.47	0.2	0.21	0.031
2-Butyl-1-octanol + N ₂ ($p \approx 7.0$ MPa)										
298.15	3.07	0.073	820.13	0.71	14.0	5.2	21.72	13	1.08	0.069
323.15	8.80	0.061	805.10	1.41	5.75	7.8	21.99	10	0.84	0.123
348.15	7.65	0.055	784.72	0.21	2.46	9.0	20.35	6.1	0.68	0.058
373.15	7.42	0.056	764.20	0.67	1.31	7.0	18.19	5.7	0.57	0.055

Table 1 (continued)

T (K)	p (MPa) ^a	x_{solute}^b	ρ_L (kg·m ⁻³)	$10^3 \cdot U_L(\rho_L)$	η_L (mPa·s)	$100 U_L(\eta_L)$	σ (mN·m ⁻¹)	$100 U_L(\sigma)$	$\Gamma_2^{(1)}$ (nm ⁻²)	$U(\Gamma_2^{(1)})$ (nm ⁻²)
423.15	7.11	0.070	721.54	0.22	0.631	3.8	15.21	3.3	0.41	0.066
473.15	7.29	0.095	676.67	0.48	0.363	6.8	11.97	1.5	0.30	0.010
573.15	7.20	0.162	566.70	1.79	0.144	4.2	5.17	4.3	0.17	0.010
2-Butyl-1-octanol+CO ₂ ($x_{\text{solute}} \approx 0.10$)										
298.15	0.74	0.101	826.26	0.43	12.1	29	25.79	6.9	0.52	0.058
323.15	1.37	0.101	806.26	0.24	4.42	30	24.08	1.1	0.44	0.162
348.15	1.46	0.101	785.51	0.20	1.97	7.1	22.40	2.7	0.37	0.021
373.15	1.71	0.101	764.35	0.68	1.18	4.4	20.01	1.1	0.41	0.038
423.15	1.94	0.101	721.23	0.69	0.532	3.9	16.57	3.7	0.30	0.032
473.15	2.18	0.101	676.63	0.11	0.340	4.1	12.61	6.2	0.23	0.058
573.15	2.61	0.101	574.30	0.88	0.155	9.2	5.77	6.7	0.13	0.006
2-Butyl-1-octanol+CO ₂ ($x_{\text{solute}} \approx 0.10$)										
298.15	1.64	0.201	830.76	1.04	9.10	25	24.34	2.7	1.04	0.128
323.15	2.35	0.201	809.98	0.46	3.45	30	22.32	3.0	0.93	0.070
348.15	2.84	0.201	788.70	0.41	1.71	12	20.48	4.7	0.83	0.158
373.15	2.97	0.201	766.77	0.66	1.08	9.8	18.07	2.4	0.73	0.077
423.15	3.66	0.201	722.46	0.22	0.506	1.5	14.77	4.1	0.59	0.093
473.15	4.07	0.201	676.24	0.79	0.306	4.5	11.19	1.3	0.44	0.051
573.15	5.09	0.201	571.08	0.34	0.142	6.5	4.32	3.4	0.25	0.029

Expanded statistical relative or absolute uncertainties ($k=2$) are included for all simulated thermophysical properties

^aThe specified pressures are obtained from the simulation in the compressed liquid phase in a canonical ensemble

^b x_{solute} refers to the gas mole fraction in simulations in the compressed liquid phase. In the simulations in VLE x_{solute} can vary slightly due to surface enrichment

investigated within the same project [15–18] and further experimental results from the literature, when available. For each property, first, the influence of the solute is discussed using the results for binary mixtures consisting of the gases H_2 , He, CH_4 , H_2O , CO, N_2 , or CO_2 dissolved in *n*-dodecane, *n*-tetracontane, or 1-dodecanol. Here, the different molecular characteristics of the solutes, e.g., molecule size, weight, or polarity, allow a systematic investigation of the influence of the solute on the properties of the mixture. To study the influence of the molecular characteristics of the solvents on the properties of the mixtures, binary mixtures based on the solutes He, N_2 , or CO_2 dissolved in solvents with a variation in the chain length, hydroxylation, or branching are discussed. Finally, results for $\Gamma_2^{(1)}$ are shown for some of the investigated binary mixtures and the influence of the surface enrichment on σ is discussed.

3.1 Liquid Viscosity

The results for η_L of binary mixtures consisting of H_2 , He, N_2 , CH_4 , H_2O , CO, or CO_2 dissolved in *n*-dodecane (left panel), 1-dodecanol (middle panel), or *n*-tetracontane (right panel) are shown in Fig. 2 as a function of T . Open and closed symbols are used to indicate different x_{solute} for systems with dissolved CH_4 , H_2O , CO,

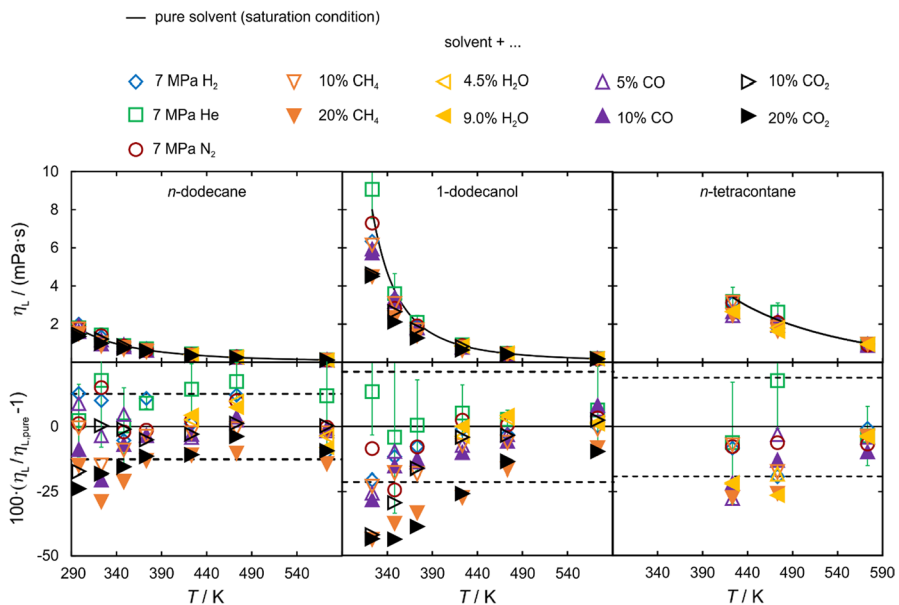


Fig. 2 (Top) Liquid dynamic viscosity η_L of the binary mixtures of *n*-dodecane (left), 1-dodecanol (middle), or *n*-tetracontane (right) with the dissolved gases H_2 , He, N_2 , CH_4 , H_2O , CO, or CO_2 by EMD simulations as a function of T and solute mole fraction (open and closed symbols). For comparison, the correlations for η_L of the solvents from EMD simulations [15] are shown (solid lines). (Bottom) Relative deviations between η_L of the binary mixtures and η_L of the pure solvents. The dotted lines mark the average expanded uncertainty ($k=2$) of the results for the pure solvents. Error bars are shown only exemplarily for the mixtures containing He for clarity. The mole fractions of the dissolved gas given in the legend are approximate values. The real composition at each T can be taken from Table 1

and CO₂. For comparison, η_L of the pure solvents investigated by EMD simulations [15] are shown as solid lines. To study the influence of the dissolved gas on η_L , the deviations of η_L for the binary mixtures from the one of the pure solvents is given in the lower part of Fig. 2. Exemplary error bars are shown only for the He-based mixtures for legibility. For all the systems investigated within this section, the average expanded statistical uncertainty ($k=2$) of η_L is 12 %.

Due to the relatively large uncertainties for η_L in the range of (10 to 20) % ($k=2$), η_L of the binary mixtures shown in Fig. 2 are mostly within combined uncertainty with η_L of the pure solvents. However, even within combined uncertainties, the T -dependent trends of the deviations between the binary mixtures and the pure solvents, which represents the influence of the dissolved gas, can be compared to previous studies for η_L of binary mixtures based on the same solutes and similar solvents as shown here. For mixtures based on n -dodecane, which is shown in the left panel of Fig. 2, the results can be compared to the work of Klein et al. [18], who investigated binary mixtures of the same solutes dissolved in n -hexadecane over the same T range and similar compositions. For the solutes He and H₂ the EMD simulations in this work predict η_L of the mixtures to be larger than that of pure n -dodecane by up to (13 and 10) % for He and H₂. This agrees with the results from SLS for the binary mixtures based on n -hexadecane, which also show η_L of the mixtures to be within combined uncertainties at $T < 423$ K and larger in comparison to pure n -hexadecane by up to (13 and 7) % for He and H₂ [18]. The results from this work also agree with the findings for the n -hexadecane-based mixtures from EMD simulations by Klein et al. [18], who also found η_L of the He- or H₂-based mixtures to be, on average, larger by approximately 10 % in comparison to pure n -hexadecane. The increase in η_L for mixtures containing He or H₂ with respect to the pure solvents can be explained by the effect of the increased p necessary to dissolve the solutes, while the pure solvents are investigated under saturation conditions or at $p=0.1$ MPa. The increase of p from saturation conditions to 7.0 MPa, for example, would lead to an increase in η_L of (9.1 or 30) % for $T=(298.15$ or $573.15)$ K [31]. For the smallest gases He and H₂, this p effect seems to be larger than the effect of the dissolved gases, which usually leads to a decrease in η_L , so that η_L for these mixtures is larger than that of pure n -dodecane.

For N₂, the EMD simulations from this work also predict η_L to be, on average, larger than that of pure n -dodecane. This agrees with the findings from SLS experiments for the binary mixture of n -hexadecane+N₂ of Klein et al. [18] only for $T > 473$ K. At smaller T , the results from SLS show η_L of the mixtures to be smaller than that of pure n -hexadecane. The failure of the EMD simulations to predict a smaller η_L for the N₂-based mixtures in comparison to the pure solvent was already seen by Klein et al. [18] for the n -hexadecane-based mixture. This suggests that this failure can be explained by the inability of the applied L-OPLS FF [13, 14] to accurately predict the properties of the pure solvents at low T . This was already seen and discussed in our previous publications as well as by other authors [15, 16, 18, 19]. The L-OPLS FF seems to overpredict the interstitial space between the solvent molecules, which is supported by a too small ρ_L [15, 19], and overpredict the attractive intermolecular interactions, which is expressed by a too large η_L [15, 19]. With respect to the binary mixtures with dissolved N₂, this means that in the EMD

simulations, the small N_2 molecules can occupy the overmuch interstitial space, which leads to a larger η_L in comparison to the pure solvent.

For the binary mixtures of *n*-dodecane and H_2O , the EMD simulations from this work predict η_L of the mixture to be within combined uncertainties with the pure solvent with an average absolute deviation of about 4 %. Based on the two investigated $x_{\text{solute}} = (0.045 \text{ and } 0.090)$, no clear influence of x_{solute} on η_L can be found. This agrees with the finding from SLS and EMD simulations for the binary mixtures of *n*-hexadecane and H_2O of Klein et al. [18], which also found no clear influence of dissolved H_2O on η_L of the solvent over the entire range of T and x_{solute} .

For the three solutes CH_4 , CO , and CO_2 , which were investigated over a wider range of x_{solute} due to their better solubility in the solvents in this work, also the strongest influence on η_L could be observed. For all three solutes, a smaller η_L of the mixtures in comparison to pure *n*-dodecane can be observed. This reduction by dissolving the solutes is most pronounced at the two lowest investigated T with deviations of about -25 % for CH_4 and CO_2 and -18 % for CO with respect to pure *n*-dodecane for the largest investigated x_{solute} . With increasing T this reduction decreases so that the deviations at $T = 573.15$ K are $(-14, 9.4, \text{ and } 0.30)$ % for CH_4 , CO_2 , and CO , respectively. Both the T -dependent trend and the absolute deviations of the mixtures from the pure solvent agree well with the findings for *n*-hexadecane-based mixtures from SLS and EMD simulations from Klein et al. [18]. For the binary mixture of *n*-dodecane and CO_2 , the results from this work can furthermore directly be compared to the experimental results of Czubinski et al. [37], who measured η_L for this binary mixture using a oscillating-piston viscometer with relative expanded experimental uncertainties ($k=2$) between $(2.0 \text{ and } 5.5)$ % in the T range between $(280.4 \text{ and } 351.3)$ K over a wide range of compositions. In the comparable T range between $(305.6 \text{ and } 351.3)$ K and $x_{\text{solute}} = 0.20$, the authors found a relative average deviation between η_L of the mixture from pure *n*-dodecane [31] of -29 %. This deviation is larger but still within combined uncertainties with the deviation found in this work, which is -19 % for T between $(298.15 \text{ and } 348.15)$ K and $x_{\text{solute}} = 0.20$. Here, this underprediction of the influence of the dissolved CO_2 on η_L can also be related to the aforementioned inability of the FF to predict the pure component properties and the interstitial space of the solvent. Similar to the explanation for the mixture of *n*-dodecane and N_2 , the overprediction of the interstitial space allows some of the CO_2 molecules to occupy this free volume in the fluid structure without interfering with the intermolecular interaction between the solvent molecules, which leads to the underprediction of the solute influence and, therefore, to an overprediction of η_L of the mixtures.

The investigation of binary mixtures consisting of the same solutes dissolved in 1-dodecanol allows an analysis of the influence of the solvent characteristics on η_L of the mixtures. Also here, the influence of the dissolved gases is investigated by calculating the deviation between η_L of the mixtures and that of pure 1-dodecanol was previously investigated by EMD simulations [15]. The absolute values for η_L for the eleven binary mixtures based on 1-dodecanol as well as the deviations from the pure solvent are shown in the middle panel in Fig. 2. For the three low-solubility gases H_2 , He , and N_2 , η_L of the binary mixtures agree within combined uncertainties with η_L of pure 1-dodecanol. This is in agreement with the findings for the mixtures

based on *n*-dodecane which suggests that the polar character of the alcohol molecule does not influence the interactions between solute and solvent molecules. The results for the mixture containing H_2 can further be compared to the results from Klein et al. [17], which investigated the binary mixture consisting of 1-hexadecanol and H_2 using SLS and EMD simulations. They also found η_L of these mixtures to be within combined uncertainties of the pure solvent. The η_L of the two binary mixtures containing H_2O are within 5 % of pure 1-dodecanol. This is, however, contradictory to the findings for mixtures consisting of H_2O dissolved in 1-hexadecanol of Klein et al. [17], where the results from SLS have shown an approximately 40 % larger η_L for the mixtures in comparison to pure 1-hexadecanol at $T=573.15$ K. The EMD simulations presented together with the SLS results, however, were not able to predict larger η_L for the mixtures [15], which agrees with the present work. Here it seems, that the combination of the modified L-OPLS FF [13, 14] and the SPC/E FF for water [38], which does not consider a T -dependent change of the FF parameters, fails to accurately predict the influence of the strong hydrogen bonds on η_L at high T .

For the three gases with a larger solubility, namely CH_4 , CO , and CO_2 , the η_L reduction in comparison to the pure solvent was found to be more pronounced in the 1-dodecanol than in *n*-dodecane at low T . The maximum deviation from the pure solvent is $-(44, 28, \text{ and } 44)$ % in 1-dodecanol and $-(29, 21, \text{ and } 42)$ % in *n*-dodecane for dissolved CH_4 , CO , and CO_2 , respectively. Since also the reduction of η_L for the binary mixtures containing the non-polar CH_4 is more pronounced in the alcohol than the alkane, the difference is most likely not related to the polarity of the solvent but rather to the much larger η_L of pure 1-dodecanol in comparison to *n*-dodecane. This means that dissolving a low-viscous solute leads to a stronger reduction in the mixture η_L when the solvent η_L is much larger at comparable compositions.

Finally, binary mixtures consisting of the same solutes, with the exception of CO_2 , dissolved in *n*-tetracontane are studied, which allows the investigation of the influence of the solvent carbon chain length on η_L of the mixtures. Due to the large melting point of *n*-tetracontane [15, 39], simulations could be performed only at $T > 423.15$ K. Results for η_L of the binary mixtures and pure *n*-tetracontane [15] as well as the deviations between η_L of the binary mixture and the pure solvent are shown in the right panel of Fig. 2. Since large reductions in η_L due to a dissolved gas are usually more pronounced at T between (298.15 and 373.15) K and because of the larger statistical uncertainties in determining η_L for large molecules, all η_L results for the binary mixture are within combined uncertainties of the pure solvents. This suggests that the influence of the carbon chain length of the solvent is rather weak. This is supported also by experimental SLS investigations of the same solutes as investigated in this work dissolved in either *n*-hexadecane [18] or *n*-octacosane [17], which showed almost identical deviations between η_L of the binary mixtures and the pure solvents in both cases.

To further study the influence of the molecular characteristics of the solvent on the thermophysical properties of the mixtures, binary systems consisting of either He, N_2 , or CO_2 dissolved in various solvents were investigated by EMD simulations. The results for η_L for the binary mixtures as well as the relative deviation from η_L of the pure solvents [15] are shown in Fig. 3 for the solutes He (left panel), N_2 (middle panel), and CO_2 (right panel).

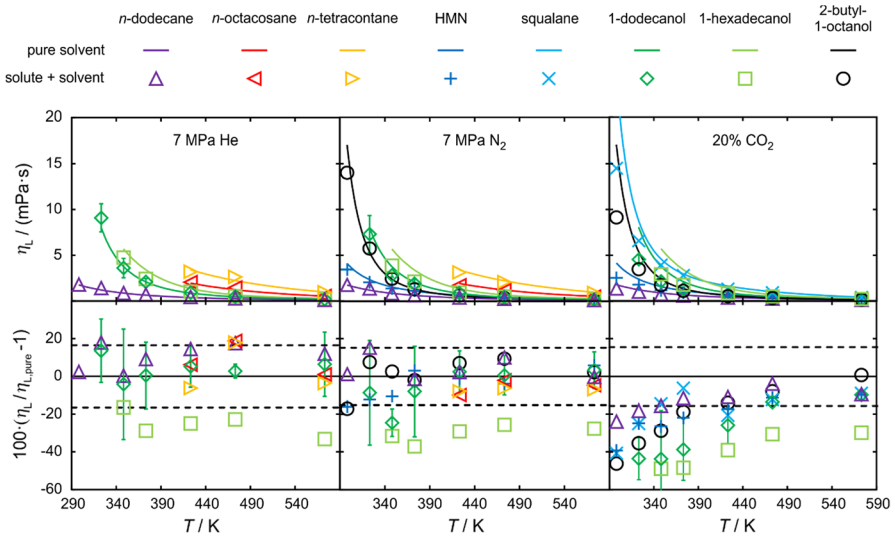


Fig. 3 (Top) Liquid dynamic viscosity η_L of the binary mixtures consisting of He (left panel), N_2 (middle panel), and CO_2 (right panel) dissolved in various solvents investigated by EMD simulations as a function of T . For comparison, η_L of the pure solvents investigated by EMD simulations [15] are shown (solid lines). (Bottom) Relative deviations of η_L of the binary mixtures from η_L of the pure solvents. The dotted lines mark the average expanded statistical uncertainty ($k=2$) of η_L for the pure solvents. Error bars are shown only exemplarily for the mixtures based on 1-dodecanol for clarity

In the case of He as the solute, η_L of the mixtures scatter around that of the pure solvents over the entire T range for most solvents. The only exception is the mixture based on 1-hexadecanol, where a (16 to 33) % smaller η_L of the mixture in comparison to pure 1-hexadecanol can be found over the entire T range. Here, it seems that the He molecules are interfering with the intermolecular interactions of 1-hexadecanol more strongly than with other solvents. This is also observed when comparing mixtures of N_2 or CO_2 dissolved in different solvents. The largest reduction in η_L can be observed for the 1-hexadecanol-based mixtures. Therefore, it seems that a failure of the solute FF can be ruled out.

Results for η_L of further binary mixtures based on N_2 as the solute show no systematic deviations from the pure solvents, which agrees with the results from EMD simulations for the binary mixture of *n*-hexadecane and N_2 from our previous investigation [18]. Here, one should keep in mind, however, that SLS results from the same publication [18] have shown that at $T < 373.15$ K a reduction in η_L in comparison to pure *n*-hexadecane could be observed, as discussed in the previous section.

Finally, investigations of binary mixtures with CO_2 as the solute and $x_{solute} = 0.20$, which are shown in the right panel of Fig. 3, show a typical T -dependent trend. There is first a strong reduction of η_L caused by adding CO_2 at low T , followed by a convergence to η_L to that of the pure solvent with increasing T . This behavior could already be seen for CO_2 dissolved in various solvents by SLS and EMD simulations [17, 18]. While the T -dependent trend is very similar for the different solvents, the magnitudes of the relative deviations change significantly with the molecular

characteristics. In general, dissolved CO_2 has a stronger impact on η_L of alcohol-based mixtures. This can be explained by the presence of strong hydrogen bond, which are partly replaced by interactions with the polar CO_2 molecules. The dispersive van-der-Waals interactions, which are present in both alkanes and alcohols, are weaker in comparison, which explains the smaller impact of dissolved CO_2 on η_L of alkane-based mixtures. The comparison between the linear 1-dodecanol and the branched 2-butyl-1-octanol as the solvent shows a stronger reduction for the linear alcohol. An explanation for this behavior can be found in the steric effect of the side branch in 2-butyl-1-octanol, which allows CO_2 molecules to occupy the free volume created by the steric effect without interfering with the intermolecular interactions between the solvent molecules.

3.2 Interfacial Tension

The interfacial tension σ was calculated using EMD simulations for the same binary mixtures and the same thermodynamic states as for η_L . In the following, the influence of the molecular characteristics of the solvent and solute on σ is investigated by comparing the results for the binary mixture with σ of the pure solvents also investigated using EMD simulations and published in a previous publication [15].

The results for σ of binary mixtures consisting of H_2 , He, N_2 , CH_4 , H_2O , CO, or CO_2 dissolved in *n*-dodecane (left panel), 1-dodecanol (middle panel), or *n*-tetracontane (right panel) are shown in Fig. 4 as function of T . Open and closed symbols are used to indicate different x_{solute} for systems with dissolved CH_4 , H_2O , CO, and CO_2 . For comparison, σ of the pure solvents investigated by EMD simulations [15] are shown as solid lines. To study the influence of the dissolved gases on σ , the deviations of σ for the binary mixtures from that of the pure solvents is given in the lower part of Fig. 4. Exemplary error bars are shown only for the He-based mixtures for legibility. The results in Fig. 4 show that due to the much smaller statistical uncertainty ($k=2$) of approximately 2.5 %, the influence of the solute on σ of the binary mixtures can be better resolved than was possible for η_L .

In the case of the solvent *n*-dodecane, the results from this work can be compared to the binary mixtures based on the same solutes and the solvent *n*-hexadecane investigated by SLS and EMD simulations [18]. For the two solutes He and H_2O , σ of the binary mixtures are within combined uncertainty of pure *n*-dodecane over the entire T range. This agrees well with the findings for the same solutes dissolved in *n*-hexadecane by SLS and EMD simulations [18]. For the solute H_2 , a smaller σ for the mixtures in comparison to pure *n*-dodecane with deviations up to 10 % were found in this work. Since both SLS and EMD simulations have shown agreement between σ for binary mixtures of H_2 dissolved in *n*-hexadecane and that of pure *n*-hexadecane, it seems that H_2 has a stronger influence on σ for shorter *n*-alkanes. A possible explanation for this, is the smaller difference between the liquid and vapor densities for shorter alkanes. Since the density difference is often used to correlate the interfacial tension [40], this can explain why dissolved H_2 seems to have a stronger influence on σ in mixtures based on shorter alkanes.

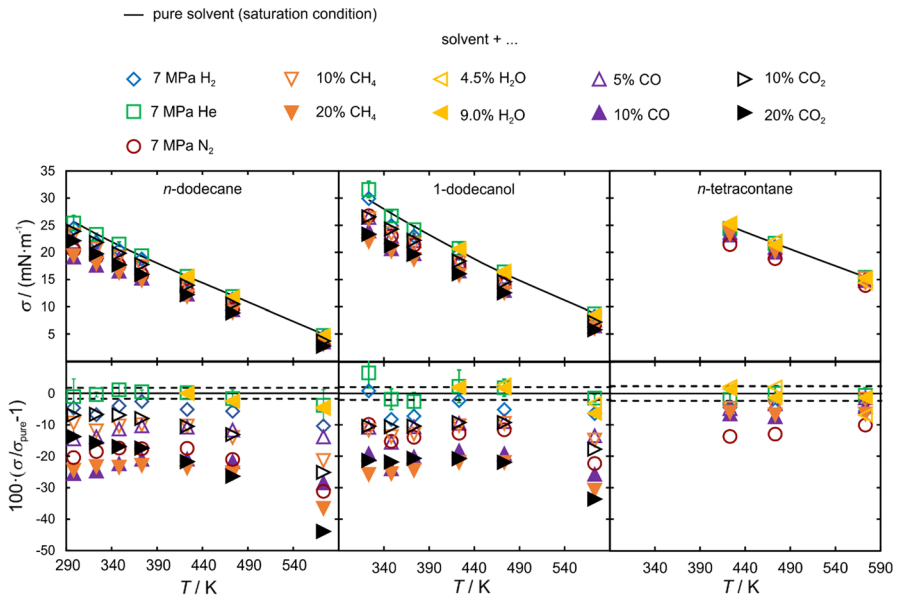


Fig. 4 (Top) Interfacial tension σ of the binary mixtures of *n*-dodecane (left), 1-dodecanol (middle), or *n*-tetracontane (right) with the dissolved gases H_2 , He, N_2 , CH_4 , H_2O , CO, or CO_2 by EMD simulations as a function of T and solute mole fraction (open and closed symbols). For comparison, the correlations for σ of the solvents from EMD simulations [15] are shown (solid lines). (Bottom) Relative deviations between σ of the binary mixtures and σ of the pure solvents. The dotted lines mark the average expanded uncertainty ($k=2$) of the results for the pure solvents. Error bars are shown only exemplarily for the mixtures containing He for clarity. The mole fractions of the dissolved gas given in the legend are approximate values. The real composition at each T can be taken from Table 1

For the more soluble gases, a clear reduction in σ is observed from the addition of the dissolved gas. This reduction grows stronger with increasing x_{solute} . The magnitude and T -dependent trend of the deviations of σ for the mixtures from pure *n*-dodecane are similar to those observed in *n*-hexadecane [18]. At $T < 473$ K, the deviation between σ of the binary mixtures and pure *n*-hexadecane are within 27 % and show only a small T -dependent trend. At $T = 573.15$ K, this deviation increases for most mixtures and reaches a maximum of approximately 44 % in the case of the binary mixture with CO_2 and $x_{\text{solute}} = 0.20$. An explanation for the larger deviations at the highest investigated T is the small absolute value for σ at this T , which leads to an increasing relative deviation in comparison to mixtures based on *n*-hexadecane, which has a larger σ [15, 41].

The relative deviations between the binary mixtures based on 1-dodecanol with the same dissolved gases as investigated in *n*-dodecane are depicted in the middle panel of Fig. 4 and show a very similar T -dependent trend as the *n*-dodecane-based mixtures. The largest difference can be found at $T = 573.15$ K, where the deviations in the 1-dodecanol-based mixtures are in general smaller in comparison to the *n*-dodecane-based mixtures. This can again be explained with the larger absolute value for σ of 1-dodecanol than *n*-dodecane. The comparison

between *n*-dodecane and 1-dodecanol as the solvents shows that the terminal hydroxyl group seems to have only a very small influence on σ in binary mixtures with dissolved gases. This can be explained by the tendency of long primary alcohols to arrange themselves in such a way at the interface that the hydroxyl group is oriented into the liquid bulk phase and the alkane tail is oriented towards the interface [15, 16, 42].

The results for σ of binary mixtures consisting of *n*-tetracontane and the same solutes, with the exception of CO₂, are shown in the right panel of Fig. 4. For the solutes He, H₂, and H₂O, agreement within combined uncertainties with σ of pure *n*-tetracontane can be found, which agrees with the observations done for the same solutes dissolved in *n*-dodecane, *n*-hexadecane [18], or *n*-octacosane [17]. For the mixtures containing CH₄, N₂, or CO, however, the reduction in σ is, in comparison to the pure solvent, much less pronounced in the *n*-tetracontane-based mixtures than in other solvents. A possible explanation for this is the molecule size or shape of *n*-tetracontane. The linear character with a very long carbon chain containing 40 carbon atoms can lead to bending and entanglement between the solvent molecules, which causes free volume within the fluid structure. This free volume can be occupied by the solute molecules and leads to a depletion of solute molecules at the vapor–liquid interface. Therefore, only a small influence of the solute on σ of the binary mixture can be observed. The larger influence of N₂ in comparison to CO or CH₄ can again be explained by the larger vapor density in the case of N₂ due to the larger p .

As it was done for η_L , the influence of the molecular characteristics of the solvent on the σ of the mixtures is addressed with the binary systems consisting of either He, N₂, or CO₂ dissolved in various solvents. The results for σ of the binary mixtures as well as the relative deviation from σ of the pure solvents [15] are shown in Fig. 5 for the solutes He (left panel), N₂ (middle panel), and CO₂ (right panel). In the case of He as the solute, no clear influence of the dissolved He on σ of the binary mixtures can be found, with the exception of the mixture containing 1-hexadecanol as the solvent. Similar to what was shown for η_L , σ of the binary mixture consisting of He dissolved in 1-hexadecanol is between (9 and 17) % smaller than that of pure 1-hexadecanol. Since there are no experimental data available for mixtures consisting of He dissolved in a primary alcohol, this behavior cannot be verified.

For the binary mixtures containing N₂ as the solvent, which are shown in the middle panel of Fig. 5, we can find a reduction in σ in comparison to the pure solvent between (10 and 31) %. Up to $T=473$ K, no clear T -dependent trend for the relative deviation between σ of the binary mixtures and that of the pure solvent can be observed. At $T=573.15$ K, the relative deviation is in general larger for mixtures where σ of the solvent is small. The fact that the relative deviation between σ of the mixtures and that of the pure solvents are very similar for the different investigated solvents shows that the molecular characteristics of the solvent, e.g., chain length, branching, or hydroxylation, have only a small influence on σ in mixtures with dissolved N₂. For mixtures based on the solute CO₂, which are shown in the right panel of Fig. 5, however, a clear influence of the solvent characteristics on σ of the mixtures can be found. While the relative deviation between σ of the mixtures and that of the pure solvent are clearly visible for all investigated solvents, the

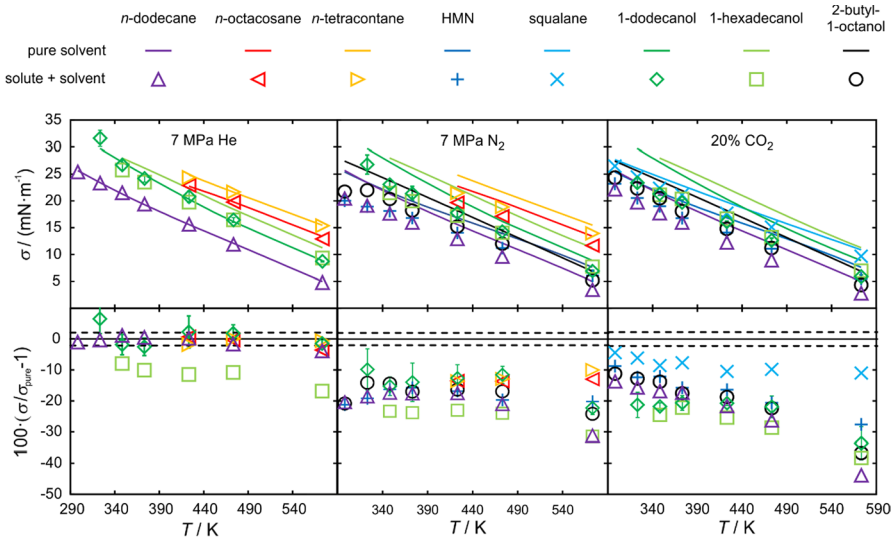


Fig. 5 (Top) Interfacial tension σ of the binary mixtures consisting of He (left panel), N₂ (middle panel), and CO₂ (right panel) dissolved in various solvents investigated by EMD simulations as a function of T . For comparison, σ of the pure solvents investigated by EMD simulations [15] are shown (solid lines). (Bottom) Relative deviations between σ of the binary mixtures from that of the pure solvents. The dotted lines mark the average expanded statistical uncertainty ($k=2$) of σ for the pure solvents. Error bars are shown only exemplarily for the mixtures based on 1-dodecanol for clarity

magnitude and T -dependent trend varies greatly. The influence of the dissolved CO₂ is less pronounced in the branched alkanes or alcohols, i.e., squalane, HMN, and 2-butyl-1-octanol, than in the linear ones. For the mixture based on squalane, for example, the deviation between σ of the mixture and that of pure squalane are within 11 %, while mixtures based on the linear isomers *n*-triacontane deviate by up to 20 % from the pure solvent. The dissolved CO₂ also seems to have a smaller influence on the branched 2-butyl-1-octanol than on the linear 1-dodecanol at $T < 423.15$ K. The smaller influence in branched molecules can be explained by the free volume in the fluid structure caused by the steric effects of the side branches. As previously mentioned, this free volume can be occupied by the solute molecules, which leads to a smaller impact of the dissolved gases on σ of the mixtures.

3.3 Structure–Property Relationship—Influence of Surface Enrichment on the Interfacial Tension

The relative adsorption of the solute (component 2) relative to the solvent (component 1) $\Gamma_2^{(1)}$ as a measurement for the enrichment of solutes molecules at the vapor–liquid interface can be used to investigate how the fluid structure close to the interface influences σ [35, 43, 44]. In this work, $\Gamma_2^{(1)}$ is used to study why different solutes with comparable x_{solute} in the bulk liquid phase have a different impact on σ . For this, the results for $\Gamma_2^{(1)}$ of binary mixtures consisting of H₂,

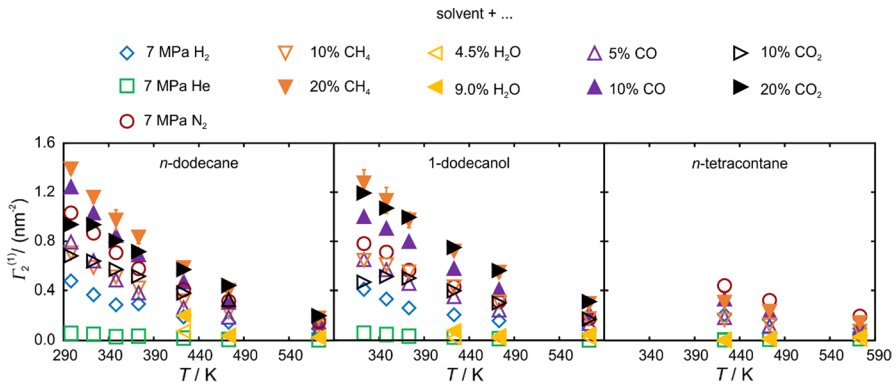


Fig. 6 Relative Adsorption of the solute (component 2) relative to the solvent (component 1) $\Gamma_2^{(1)}$ of the binary mixtures of *n*-dodecane (left), 1-dodecanol (middle), or *n*-tetracontane (right) with the dissolved gases H₂, He, N₂, CH₄, H₂O, CO, or CO₂ by EMD simulations as a function of *T* and solute mole fraction (open and closed symbols). Error bars are shown only exemplarily for the mixtures containing CH₄ and $x_{\text{solute}} = 0.20$ for clarity. The mole fractions of the dissolved gas given in the legend are approximate values. The real composition at each *T* can be taken from Table 1

He, N₂, CH₄, H₂O, CO, or CO₂ dissolved in *n*-dodecane (left panel), 1-dodecanol (middle panel), or *n*-tetracontane (right panel) are shown in Fig. 6 as function of *T*. Open and closed symbols are used to indicate different x_{solute} for systems with dissolved CH₄, H₂O, CO, and CO₂.

The results in Fig. 6 for all three solvents show a general decrease of $\Gamma_2^{(1)}$ with increasing *T*. This can be explained by the increasing kinetic energy and dynamics of the molecules, which counteracts the enrichment of the solute molecules at the vapor–liquid interface by the mixing process. For all three investigated solvents, $\Gamma_2^{(1)}$ for the mixtures containing H₂O and He are close to zero, indicating that there is no or only a very small enrichment of the solute molecules at the interface. This is not surprising, since also σ for these systems are mostly within combined uncertainties with that of the pure solvents. Also for the solute H₂, only small $\Gamma_2^{(1)}$ within 0.5 nm⁻² can be found in all three solvents. This agrees well with the value found for the binary mixtures consisting of *n*-hexadecane with dissolved H₂ were $\Gamma_2^{(1)} = 0.54 \text{ nm}^{-2}$ was calculated for $T = 323.15 \text{ K}$ [18]. A large difference in $\Gamma_2^{(1)}$ can be found, for example, when comparing the solutes CH₄, CO, and CO₂ dissolved in either *n*-dodecane or 1-dodecanol at $x_{\text{solute}} = 0.10$. Here, $\Gamma_2^{(1)}$ of the mixtures containing CO is approximately 50 % larger than that of the other two solutes at $T = 298.15 \text{ K}$, indicating a larger surface enrichment of CO. This observation can explain why σ of the binary mixture containing CO deviate more from σ of the pure solvent, as shown in Fig. 4. In the case of *n*-tetracontane, the largest $\Gamma_2^{(1)}$ can be found for the mixture containing N₂, which agrees with the observations from the investigation of σ , where the largest deviation between σ of the mixtures and that of pure *n*-tetracontane was found for the mixture containing N₂. Additionally, the smaller influence of dissolved CH₄ on σ in mixtures based on *n*-tetracontane in comparison to other linear alkanes can directly be linked to the smaller $\Gamma_2^{(1)}$ in *n*-tetracontane-based mixtures.

In general, the results for $\Gamma_2^{(1)}$ shown in Fig. 6 and given in Table 1 show that the deviation between σ of the binary mixtures from that of the pure solvents are inversely proportional to $\Gamma_2^{(1)}$, which shows that the enrichment of solute molecules at the vapor–liquid interface is an important property for understanding, correlating, and predicting σ of mixtures consisting of liquids with dissolved gases [35, 43, 44].

4 Conclusions

In the present study, results for η_L , σ , and $\Gamma_2^{(1)}$ of 45 binary mixtures consisting of a linear, branched, or oxygenated hydrocarbon and a dissolved gas obtained by EMD simulations are presented. The binary mixtures consist of the solvents *n*-dodecane, *n*-octacosane, *n*-tetracontane, HMN, squalane, 1-dodecanol, 1-hexadecanol, or 2-butyl-1-octanol and the solutes H₂, He, CH₄, H₂O, N₂, CO, or CO₂ and were investigated in the *T* range between (298.15 and 573.15) K and x_{solute} up to 0.20. Using EMD simulations, η_L , σ , and $\Gamma_2^{(1)}$ of the binary mixtures could be accessed with average expanded statistical uncertainties ($k=2$) of (12, 3.7, and 12) %, respectively. By comparing the thermophysical properties of the binary mixtures with those of the pure solvents, the influence of the dissolved gas on η_L and σ could be analyzed. Due to the relatively large statistical uncertainties for η_L , such an influence could not be resolved within combined uncertainties of the binary mixture and the pure solvent data. For the more soluble gases CH₄, CO, or CO₂, however, an influence of the dissolved gas could be pointed out and the results were compared to those obtained by SLS and EMD simulations for binary mixtures with similar solvents and the same dissolved gases. Here, deviations of up to –50 % with respect to η_L of the pure solvent could be observed for binary mixtures containing CH₄ or CO₂ at *T* between (298.15 and 323.15) K. With increasing *T*, the difference between η_L of the mixtures and that of the pure solvents reduced for all binary mixtures based on these solutes and was mostly within combined uncertainties at *T*=573.15 K. For the solute CO, a similar *T*-dependent trend for the difference between η_L of the mixtures and that of the pure solvents was observed. However, the relative deviation was always within 27 % and, therefore, always smaller in comparison to the mixtures containing CH₄ or CO₂. An investigation of the solutes He, N₂, or CO₂ in different solvents has shown that the relative reduction of η_L in comparison to the pure solvents is larger in mixtures containing linear or branched alcohols than in linear or branched alkanes. The observations with respect to the influence of the gas on η_L agree well with experimental and simulated data for binary mixtures based on similar solvents from the literature.

In the case of σ , the relatively small statistical uncertainties allowed a more thorough analysis of the influence of the dissolved gases for all binary mixtures. While σ of mixtures containing the solutes He or H₂O are mostly within uncertainties of the pure solvents, large deviations outside combined uncertainties were found for CH₄, CO, or CO₂ over the entire *T* range. Here, the influence of the dissolved gas was found to strongly depend on the solute type. The binary mixture of CO dissolved in *n*-dodecane with $x_{\text{solute}}=0.10$, for example, deviates by –27 % from σ of

pure *n*-dodecane at $T = 298.15$ K, while the mixtures with dissolved CO_2 at the same T and x_{solute} deviates only by approximately -8% . With the help of $\Gamma_2^{(1)}$, which could also be calculated from EMD simulations in VLE, the stronger impact of CO on σ could be related to its stronger enrichment at the vapor–liquid interface. Although absolute values for η_L and σ can differ by up to 30% , the agreement between experimental and simulated results shows that EMD simulations are a valuable tool for the prediction of how a dissolved gas may influence mixture properties.

Supplementary Information The online version contains supplementary material available at <https://doi.org/10.1007/s10765-022-03038-5>.

Acknowledgements This work was financially supported by the German Research Foundation (Deutsche Forschungsgemeinschaft, DFG) via the project Grants FR 1709/15-1. The authors gratefully acknowledge funding of the Erlangen Graduate School in Advanced Optical Technologies (SAOT) by the Bavarian State Ministry for Science and Art and further gratefully acknowledge the computing resources and support provided by the Erlangen Regional Computing Center (RRZE).

Funding Open Access funding enabled and organized by Projekt DEAL.

Declarations

Conflict of interest The authors have no competing interests to declare that are relevant to the content of this article.

Open Access This article is licensed under a Creative Commons Attribution 4.0 International License, which permits use, sharing, adaptation, distribution and reproduction in any medium or format, as long as you give appropriate credit to the original author(s) and the source, provide a link to the Creative Commons licence, and indicate if changes were made. The images or other third party material in this article are included in the article's Creative Commons licence, unless indicated otherwise in a credit line to the material. If material is not included in the article's Creative Commons licence and your intended use is not permitted by statutory regulation or exceeds the permitted use, you will need to obtain permission directly from the copyright holder. To view a copy of this licence, visit <http://creativecommons.org/licenses/by/4.0/>.

References

1. B. Li, K.-J. Jens, *Ind. Eng. Chem. Res.* **53**, 1735 (2014). <https://doi.org/10.1021/ie401966w>
2. S. Lee, A. Sardesai, *Top. Catal.* **32**, 197 (2005). <https://doi.org/10.1007/s11244-005-2891-8>
3. S. Lee, M.R. Gogate, C.J. Kulik, *Chem. Eng. Sci.* **47**, 3769 (1992). [https://doi.org/10.1016/0009-2509\(92\)85096-T](https://doi.org/10.1016/0009-2509(92)85096-T)
4. A.P. Kulkarni, T. Hos, M.V. Landau, D. Fini, S. Giddey, M. Herskowitz, *Sustain. Energy Fuels* **5**, 486 (2021). <https://doi.org/10.1039/D0SE01125H>
5. C.V. Rode, A. Bhattacharya, R.V. Chaudhari, *Can. J. Chem. Eng.* **70**, 612 (1992). <https://doi.org/10.1002/cjce.5450700330>
6. C.J. Stacy, C.A. Melick, R.A. Cairncross, *Fuel Process. Technol.* **124**, 70 (2014). <https://doi.org/10.1016/j.fuproc.2014.02.003>
7. M.P. Allen, D.J. Tildesley, *Computer Simulation of Liquids* (Oxford University Press, New York, 1987)
8. D. Frenkel, B. Smit, *Understanding Molecular Simulation: From Algorithms to Applications* (Academic Press, San Diego, 2002)
9. D.C. Rapaport, *The Art of Molecular Dynamics Simulation*, 2nd edn. (Cambridge University Press, Cambridge, 2004)

10. C. Giraudet, T. Klein, G. Zhao, M.H. Rausch, T.M. Koller, A.P. Fröba, J. Phys. Chem. B **122**, 3163 (2018). <https://doi.org/10.1021/acs.jpcc.8b00733>
11. W. Wu, T. Klein, M. Kerscher, M.H. Rausch, T.M. Koller, C. Giraudet, A.P. Fröba, J. Phys. Chem. B **123**, 8777 (2019). <https://doi.org/10.1021/acs.jpcc.9b06211>
12. M. Piszko, F.D. Lenahan, S. Hahn, M.H. Rausch, T.M. Koller, T. Klein, A.P. Fröba, J. Chem. Eng. Data **66**, 2218 (2021). <https://doi.org/10.1021/acs.jced.1c00084>
13. S.W.I. Siu, K. Pluhackova, R.A. Böckmann, J. Chem. Theory Comput. **8**, 1459 (2012). <https://doi.org/10.1021/ct200908r>
14. K. Pluhackova, H. Morhenn, L. Lautner, W. Lohstroh, K.S. Nemkovski, T. Unruh, R.A. Böckmann, J. Phys. Chem. B **119**, 15287 (2015). <https://doi.org/10.1021/acs.jpcc.5b08569>
15. T. Klein, F.D. Lenahan, M. Kerscher, M.H. Rausch, I.G. Economou, T.M. Koller, A.P. Fröba, J. Phys. Chem. B **124**, 4146 (2020). <https://doi.org/10.1021/acs.jpcc.0c01740>
16. F.D. Lenahan, M. Zikeli, M.H. Rausch, T. Klein, A.P. Fröba, J. Chem. Eng. Data **66**, 2264 (2021). <https://doi.org/10.1021/acs.jced.1c00108>
17. T. Klein, F.D. Lenahan, Z. Zhai, M. Kerscher, J.H. Jander, T.M. Koller, M.H. Rausch, A.P. Fröba. Int. J. Thermophys. (2022) (accepted for publication)
18. T. Klein, F.D. Lenahan, M. Kerscher, J.H. Jander, M.H. Rausch, T.M. Koller, A.P. Fröba, J. Chem. Eng. Data **66**, 3205 (2021). <https://doi.org/10.1021/acs.jced.1c00289>
19. K.D. Papavasileiou, L.D. Peristeras, A. Bick, I.G. Economou, J. Phys. Chem. B **123**, 6229 (2019). <https://doi.org/10.1021/acs.jpcc.9b02840>
20. O.A. Moulτος, I.N. Tsimpanogiannis, A.Z. Panagiotopoulos, J.P.M. Trusler, I.G. Economou, J. Phys. Chem. B **120**, 12890 (2016). <https://doi.org/10.1021/acs.jpcc.6b04651>
21. W. Wu, T. Klein, M. Kerscher, M.H. Rausch, T.M. Koller, C. Giraudet, A.P. Fröba, J. Phys. Chem. B **124**, 2482 (2020). <https://doi.org/10.1021/acs.jpcc.0c00646>
22. T. Klein, W. Wu, M.H. Rausch, C. Giraudet, T.M. Koller, A.P. Fröba, J. Phys. Chem. B **122**, 7122 (2018). <https://doi.org/10.1021/acs.jpcc.8b03568>
23. M. Kerscher, T. Klein, P.S. Schulz, E. Veroutis, S. Dürr, P. Preuster, T.M. Koller, M.H. Rausch, I.G. Economou, P. Wasserscheid, A.P. Fröba, Int. J. Hydrog. Energy **45**, 28903 (2020). <https://doi.org/10.1016/j.ijhydene.2020.07.261>
24. P.S. Schmidt, M. Kerscher, T. Klein, J.H. Jander, F.E. Berger Bioucas, T. Rüde, S. Li, M. Stadelmaier, S. Hanyon, R.R. Fathalla, A. Bösmann, P. Preuster, P. Wasserscheid, T.M. Koller, M.H. Rausch, A.P. Fröba. Int. J. Hydrogen Energy **47**, 6111 (2022). <https://doi.org/10.1016/j.ijhydene.2021.11.198>
25. M.J. Abraham, T. Murtola, R. Schulz, S. Páll, J.C. Smith, B. Hess, E. Lindahl, SoftwareX **1–2**, 19 (2015). <https://doi.org/10.1016/j.softx.2015.06.001>
26. B. Hess, H. Bekker, H.J.C. Berendsen, J.G.E.M. Fraaije, J. Comput. Chem. **18**, 1463 (1997). [https://doi.org/10.1002/\(SICI\)1096-987X\(199709\)18:12%3c1463::AID-JCC4%3e3.0.CO;2-H](https://doi.org/10.1002/(SICI)1096-987X(199709)18:12%3c1463::AID-JCC4%3e3.0.CO;2-H)
27. T. Darden, D. York, L. Pedersen, J. Chem. Phys. **98**, 10089 (1993). <https://doi.org/10.1063/1.464397>
28. C.L. Wennberg, T. Murtola, S. Páll, M.J. Abraham, B. Hess, E. Lindahl, J. Chem. Theory Comput. **11**, 5737 (2015). <https://doi.org/10.1021/acs.jctc.5b00726>
29. M.S. Green, J. Chem. Phys. **22**, 398 (1954). <https://doi.org/10.1063/1.1740082>
30. R. Kubo, J. Phys. Soc. Jpn. **12**, 570 (1957). <https://doi.org/10.1143/JPSJ.12.570>
31. E.W. Lemmon, I.H. Bell, M.L. Huber, M.O. McLinden, REFPROP, Standard Reference Data Program. Version 10.0. (National Institute of Standards and Technology, Gaithersburg, MD, USA, 2018)
32. Z.A. Makrodimitri, A. Heller, T.M. Koller, M.H. Rausch, M.S.H. Fleys, A.N.R. Bos, G.P. van der Laan, A.P. Fröba, I.G. Economou, J. Chem. Thermodyn. **91**, 101 (2015). <https://doi.org/10.1016/j.jct.2015.07.026>
33. Y. Zhang, A. Otani, E.J. Maginn, J. Chem. Theory Comput. **11**, 3537 (2015). <https://doi.org/10.1021/acs.jctc.5b00351>
34. T.M. Koller, S. Yan, C. Steiningger, T. Klein, A.P. Fröba, Int. J. Thermophys. **40**, 79 (2019). <https://doi.org/10.1007/s10765-019-2544-y>
35. S. Stephan, H. Hasse, Int. Rev. Phys. Chem. **39**, 319 (2020). <https://doi.org/10.1080/0144235X.2020.1777705>
36. M.M. Telo da Gama, R. Evans, Mol. Phys. **48**, 229 (1983). <https://doi.org/10.1080/00268978300100181>
37. F.F. Czubinski, C.J. Noriega Sanchez, A.K. da Silva, M.A. Marcelino Neto, J.R. Barbosa. J. Chem. Eng. Data **64**, 3375 (2019) <https://doi.org/10.1021/acs.jced.9b00187>

38. H.J.C. Berendsen, J.R. Grigera, T.P. Straatsma, *J. Phys. Chem.* **91**, 6269 (1987). <https://doi.org/10.1021/j100308a038>
39. A. Heller, M.S.H. Fleys, J. Chen, G.P. van der Laan, M.H. Rausch, A.P. Fröba, *J. Chem. Eng. Data* **61**, 1333 (2016). <https://doi.org/10.1021/acs.jced.5b00986>
40. T.M. Koller, C. Steininger, M.H. Rausch, A.P. Fröba, *Int. J. Thermophys.* **38**, 167 (2017). <https://doi.org/10.1007/s10765-017-2301-z>
41. T. Klein, S. Yan, J. Cui, J.W. Magee, K. Kroenlein, M.H. Rausch, T.M. Koller, A.P. Fröba, *J. Chem. Eng. Data* **64**, 4116 (2019). <https://doi.org/10.1021/acs.jced.9b00525>
42. C.D. Stanners, Q. Du, R.P. Chin, P. Cremer, G.A. Somorjai, Y.R. Shen, *Chem. Phys. Lett.* **232**, 407 (1995). [https://doi.org/10.1016/0009-2614\(94\)01362-Y](https://doi.org/10.1016/0009-2614(94)01362-Y)
43. S. Becker, S. Werth, M. Horsch, K. Langenbach, H. Hasse, *Fluid Phase Equilib.* **427**, 476 (2016). <https://doi.org/10.1016/j.fluid.2016.08.007>
44. S. Stephan, D. Schaefer, K. Langenbach, H. Hasse, *Mol. Phys.* (2021). <https://doi.org/10.1080/00268976.2020.1810798>

Publisher's Note Springer Nature remains neutral with regard to jurisdictional claims in published maps and institutional affiliations.

Authors and Affiliations

Chathura J. Kankanamge¹ · Frances D. Lenahan¹ · Tobias Klein¹  ·
Andreas P. Fröba¹

✉ Tobias Klein
tobias.klein@fau.de

¹ Department of Chemical and Biological Engineering (CBI) and Erlangen Graduate School in Advanced Optical Technologies (SAOT), Institute of Advanced Optical Technologies – Thermophysical Properties (AOT-TP), Friedrich-Alexander-Universität Erlangen-Nürnberg (FAU), Paul-Gordan-Straße 8, 91052 Erlangen, Germany